NASA TM-79712

NASA

Technical Memorandum 79712

A Rocket Ozonesonde for Geophysical Research and Satellite Intercomparisons

Ernest Hilsenrath, Robert L. Coley,
Peter T. Kirschner, and Bill Gammill

30

MARCH 1979

National Aeronautics and
Space Administration

Goddard Space Flight Center
Greenbelt, Maryland 20771

BIBLIOGRAPHIC DATA SHEET

1. Report No.	2 Government Accession No	3. Recipient's Catalog No.
4. Title and Subtitle A Rocket Ozonesonde for Geophysical Research and Satellite Intercomparisons		5. Report Date 6. Performing Organization Code 912
7. Author(s) E Hilsenrath, R Coley, P. T Kirschner, B Gammill		8. Performing Organization Report No.
9 Performing Organization Name and Address Laboratory for Atmospheric Science Goddard Space Flight Center Greenbelt, MD 20771		10. Work Unit No. 11. Contract or Grant No. 13. Type of Report and Period Covered TM
12. Sponsoring Agency Name and Address NASA Goddard Space Flight Center Greenbelt, MD 20771		14. Sponsoring Agency Code NASA

15. Supplementary Notes

16 Abstract

The in-situ rocketsonde for ozone profile measurements developed and flown for geophysical research and satellite comparison is reviewed The measurement principle involves the chemiluminescence caused by ambient ozone striking a detector and passive pumping as a means of sampling the atmosphere as the sonde descends through the atmosphere on a parachute The sonde is flown on a meteorological sounding rocket, and flight data are telemetered via the standard meteorological GMD ground receiving system. The payload operation, sensor performance, and calibration procedures simulating flight conditions are described An error analysis indicates an absolute accuracy of about 12 percent and a precision of about 8 percent These are combined to give a measurement error of 14 percent

Approximately 20 flights have been conducted for geophysical experiments, such as, during the polar night, day and night to determine diurnal variability, and during geomagnetic events Some flights were conducted for comparison with other rocket and satellite soundings for ozone In general, these comparisons showed good agreement Two nearly simultaneous soundings of the system described here showed a repeatability of 6 percent Ozone profiles measured under varying geophysical conditions, such as, during the polar and equatorial night, and at midlatitudes over a period of several years are discussed, and can be compared with ozone profiles calculated by photochemical models The polar night soundings show large variations which are indicative of the variability of the temperature and winds observed at high latitudes in winter Ozone profiles obtained at low and midlatitudes are systematically higher above 40 km than those predicted by photochemical models with complete photochemistry

17 Key Words (Selected by Author(s))	18 Distribution Statement
OZONE, UPPER ATMOSPHERE, ROCKET TECHNIQUE, DATA INTERPRETATION	

19 Security Classif (of this report)	20 Security Classif (of this page)	21. No of Pages	22. Price*

*For sale by the National Technical Information Service, Springfield, Virginia 22151

A ROCKET OZONESONDE FOR GEOPHYSICAL RESEARCH AND SATELLITE INTERCOMPARISONS

Ernest Hilsenrath
Robert L Coley
Laboratory for Atmospheric Science
Goddard Space Flight Center
Greenbelt, MD 20771

Peter T Kirschner
Astromet Plant
Thiokol Corporation
Ogden, Utah 84403

Bill Gammill
Physical Science Laboratory
New Mexico State University
Las Cruces, New Mexico 88001

GODDARD SPACE FLIGHT CENTER
Greenbelt, Maryland

This Page Intentionally Left Blank

A ROCKET OZONESONDE FOR GEOPHYSICAL RESEARCH AND SATELLITE INTERCOMPARISONS

Ernest Hilsenrath, Robert L. Coley, Peter T. Kirschner, and Bill Gammill

ABSTRACT

The in-situ rocketsonde for ozone profile measurements developed and flown for geophysical research and satellite comparison is reviewed. The measurement principle involves the chemiluminescence caused by ambient ozone striking a detector and passive pumping as a means of sampling the atmosphere as the sonde descends through the atmosphere on a parachute. The sonde is flown on a meteorological sounding rocket, and flight data are telemetered via the standard meteorological GMD ground receiving system The payload operation, sensor performance, and calibration procedures simulating flight conditions are described. An error analysis indicates an absolute accuracy of about 12 percent and a precision of about 8 percent. These are combined to give a measurement error of 14 percent.

Approximately 20 flights have been conducted for geophysical experiments, such as, during the polar night, day and night to determine diurnal variability, and during geomagnetic events. Some flights were conducted for comparison with other rocket and satellite soundings for ozone. In general, these comparisons showed good agreement Two nearly simultaneous soundings of the system described here showed a repeatability of 6 percent Ozone profiles measured under varying geophysical conditions, such as, during the polar and equatorial night, and at midlatitudes over a period of several years as discussed, and can be compared with ozone profiles calculated by photochemical models. The polar night soundings show large variations which are indicative of the variability of the temperature and winds observed at high latitudes in winter. Ozone profiles obtained at low and midlatitudes are systematically higher above 40 km than those predicted by photochemical models with complete photochemistry

This Page Intentionally Left Blank

CONTENTS

		Page
I.	INTRODUCTION	1
II.	MEASUREMENT PRINCIPLE	3
	A. Chemiluminescent Reaction	3
	1. Mechanism	5
	2. Specificity	5
	3. Chemiluminescent Disc Preparation	7
	4. Response Time	8
	B. Air Sampling Technique	9
	1. Sampling Principle	9
	2. Flow Rates in Flight	11
III.	INSTRUMENTATION	14
IV.	CALIBRATION	19
V.	ERROR ANALYSIS	24
	A. Random Flight Errors	24
	B. Systematic Errors for a Given Sounding	25
	C Absolute Errors	28
VI.	DISCUSSION OF FLIGHT DATA	35
	A. Daytime Stratospheric and Mesospheric Ozone at Midlatitudes	36
	B. Nighttime Stratospheric and Mesospheric Ozone at Low Latitudes	37
	C Stratospheric and Mesospheric Ozone in the Polar Night	38
VII	CONCLUSION AND SUMMARY	44
	REFERENCES	46
	APPENDICES	
	A Ozone Detector Preparation	49
	B Black Anodization Procedure	50
	C Telemetry System	51

1 INTRODUCTION

Early interest in stratospheric ozone was to utilize the ozone data as a tracer for the general circulation of the lower stratosphere It was soon evident that ozone was also important to the chemical and radiative properties of the upper stratosphere and lower mesosphere. Contemporary photochemical-radiative-dynamic models now demonstrate the complex interaction of ozone with other geophysical parameters, such as, tropospheric dynamics, local temperature, other atmospheric constituents, direct and indirect effects caused by solar variability, and possible anthropogenic sources

Measurements of the vertical distribution of ozone to 30 km began around 1955. Around 1960, a loose network of balloon ozonesonde stations began performing regular soundings. These data provide a basis for the ozone climatology as we know it today, though the network suffers from a lack of spatial and temporal consistency, and contains calibration and intercalibration uncertainties. Rocket soundings of ozone began in the late 1960's, and to date there are about 200 measurements in the lower mesosphere and upper stratosphere. Most of these have occurred in the United States (1, 2, 3, 4), while other soundings have been conducted from Japan (5), Sweden (6), Australia (7), and India (8) These measurements provide observational evidence of the inadequacy of Chapman photochemistry and the need for additional odd oxygen sinks predicted by contemporary photochemical models Accurate measurements of the ozone vertical distribution have taken on new importance because the predicted losses by the chlorofluoromethanes (CFM's) catalytic cycle is greatest at 40 km (9) NASA has recently established monthly rocket soundings from three sites using an optical ozonesonde (10) to build a data base of upper stratospheric ozone profiles

The vertical distribution of ozone (as well as the total columnar amount) is also being measured from satellites (11) These observations are providing a new perspective on the ozone fields

because of their near-global coverage. They do have limitations, however, because of uncertainties of the inversion techniques, satellite instrument degradation while in orbit, altitude and spatial resolution, and time/spatial resolution because of the fixed satellite orbit.

The rocket sonde described here measures ozone directly and has high accuracy and fine altitude resolution. The measurements can be implemented quickly to investigate short-term changes and can be coordinated with other direct measurements of atmospheric properties to give a complete picture of the atmospheric process being investigated. The rocket sonde complements the satellite sounders in providing comparison data and for conducting geophysical experiments which cannot be performed from orbit.

This paper reviews the overall status of the chemiluminescent rocket ozonesonde. The principle of operation is discussed in light of recent laboratory experiments. A description of the hardware includes sensor and payload operation on a meteorological rocket. The calibration procedure, its applicability to flight, and an error analysis is discussed Examples of ozone profiles are shown to demonstrate precision and comparability with other measurements from 1968 to 1975 Finally ozone profile data from measurements at midlatitudes and during the polar and tropical nighttime are presented as comparison data for photochemical models

II. MEASUREMENT PRINCIPLE

The measurement technique employs the chemiluminescent reaction of rhodamine-B dye and ozone. The ambient air is sampled by the ozone detector as the sonde descends through the atmosphere on a parachute. The chemiluminescent reaction is detected by a photometer, and the flow rate is determined by an on-board pressure gauge. The basic elements of the ozone sensor are shown in block diagram form in Figure 1 and is referred to again later. The ozonesonde consists of the ozone sensor, telemetry system, and a parachute decelerator. The ozone payload consists of the ozonesonde, nose cone, and separation system. This section covers a discussion of the chemiluminescent reaction and the air sampling principle. The succeeding section gives more details on the hardware and engineering aspects of the payload. The initial experiments utilizing this technique were described by Hilsenrath, et. al (4) and the following discussion summarizes new results since that time.

A. Chemiluminescent Reaction

The chemiluminescent technique for ozone detection was described by Beronose and Rene in 1959 (12). They demonstrated a quantitative ozone measurement capability using the oxyluminescence of certain organic compounds impregnated on paper discs. Regener (13) in 1964, using rhodamine-B dye absorbed on silica gel, developed a balloon ozonesonde compatible with the meteorological radio sonde. Subsequently, both Randhawa (2) and Hilsenrath, et. al (4) developed rocket sondes utilizing this technique However, Herring, et. al (14) and Komhyr, et. al. (15) have noted instabilities and nonlinearities in balloon flight data where the Regener sonde was used. As will be shown, the uncertainties associated with the Regener balloon sonde are virtually eliminated in the present instrument This has been accomplished by a newly developed extensive calibration procedure employed for each flight and by the added stability of the chemiluminescent detector used here

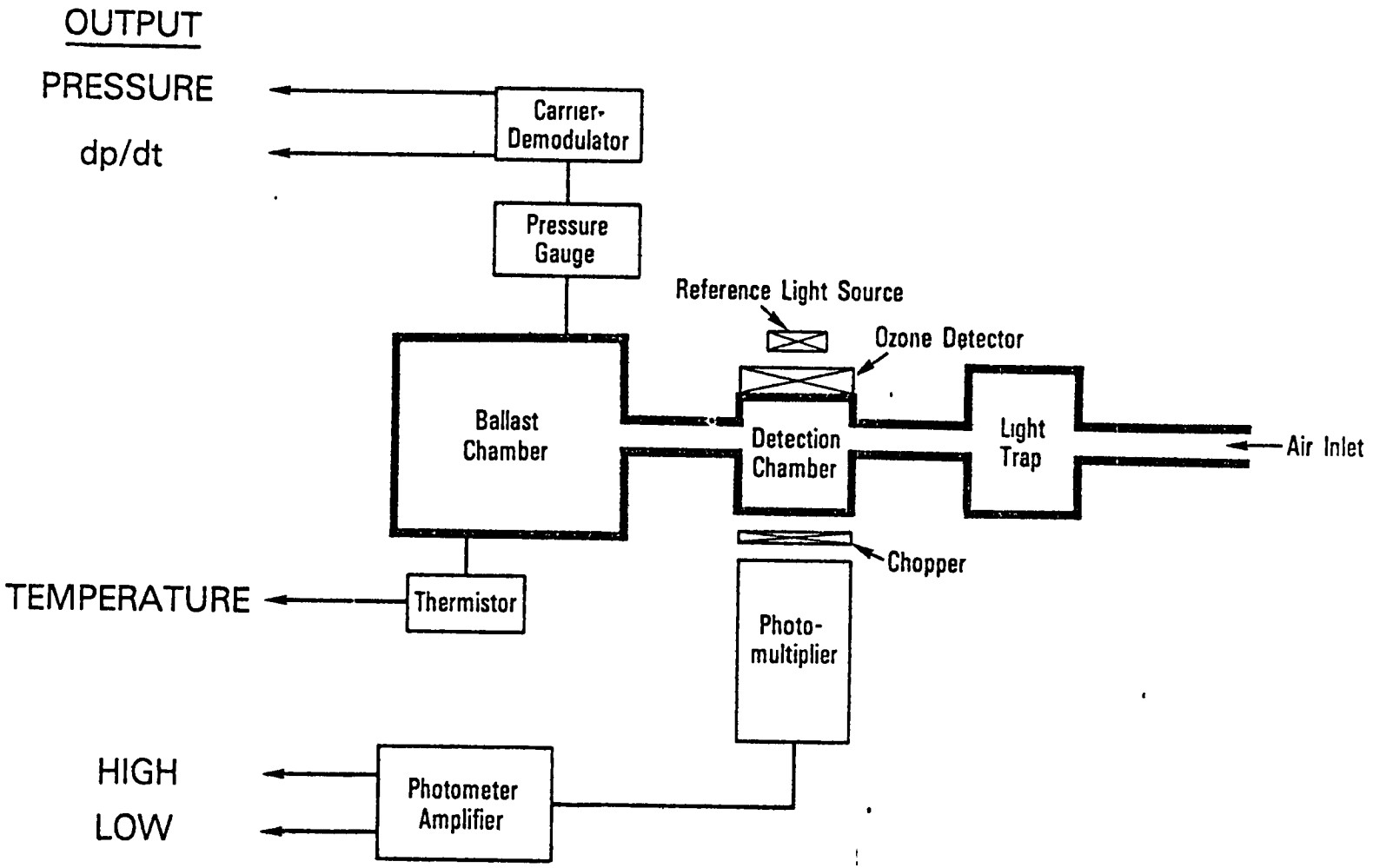

Figure 1. Ozone sensor block diagram

1. Mechanism

The chemiluminescent mechanism has been explored in the laboratory, however, it has never been fully explained. Laboratory measurements indicate that the reaction of ozone with the chemiluminescent material and the production of light has several steps. 1) adsorption of ozone, 2) catalytic decomposition, 3) liberation of energy, 4) energy transport to the disc material and to the rhodamine-B dye, 5) excitation of rhodamine-B dye, and 6) luminescence. The adsorption of ozone, the first step, depends on several factors including flow rate, pressure (diffusion rates), and detector volume geometry. These factors will be discussed in more detail in Section B. Regarding steps 2, 3, and 4, laboratory experiments show that the chemiluminescent efficiency is the same for several ozone concentrations at any flow rate and at fixed pressures. This would suggest a first order reaction. The reality of steps 5 and 6 can be verified from the chemiluminescent spectrum. Using a series of yellow and red sharp-cut off filters, a spectrum was obtained (16) and is shown in Figure 2. The emission spectrum in arbitrary units peaks near 580 nm, and is similiar to that for rhodamine-B fluorescence in solution

The left ordinate of Figure 2 gives the absolute spectral irradiance of a radioactive self-luminous light source which is spectrally similar to the chemiluminescence, and yields a signal comparable to the chemiluminescence measured by the ozone sensor photometer. The wavelength integrated irradiance is 2.35×10^{-12} watts/cm^2, which is representative of expected light levels during flight, and provides a basis for the photometer design. A photon yield of 1×10^{-5} per molecule of ozone computed from the measured irradiance resulting from a known ozone flux is a measure of the chemiluminescent efficiency.

2 Specificity

Accurate measurements require that the chemiluminescence is specific to ozone Reaction to other atmospheric constituents would make the flight results difficult to interpret. This difficulty is

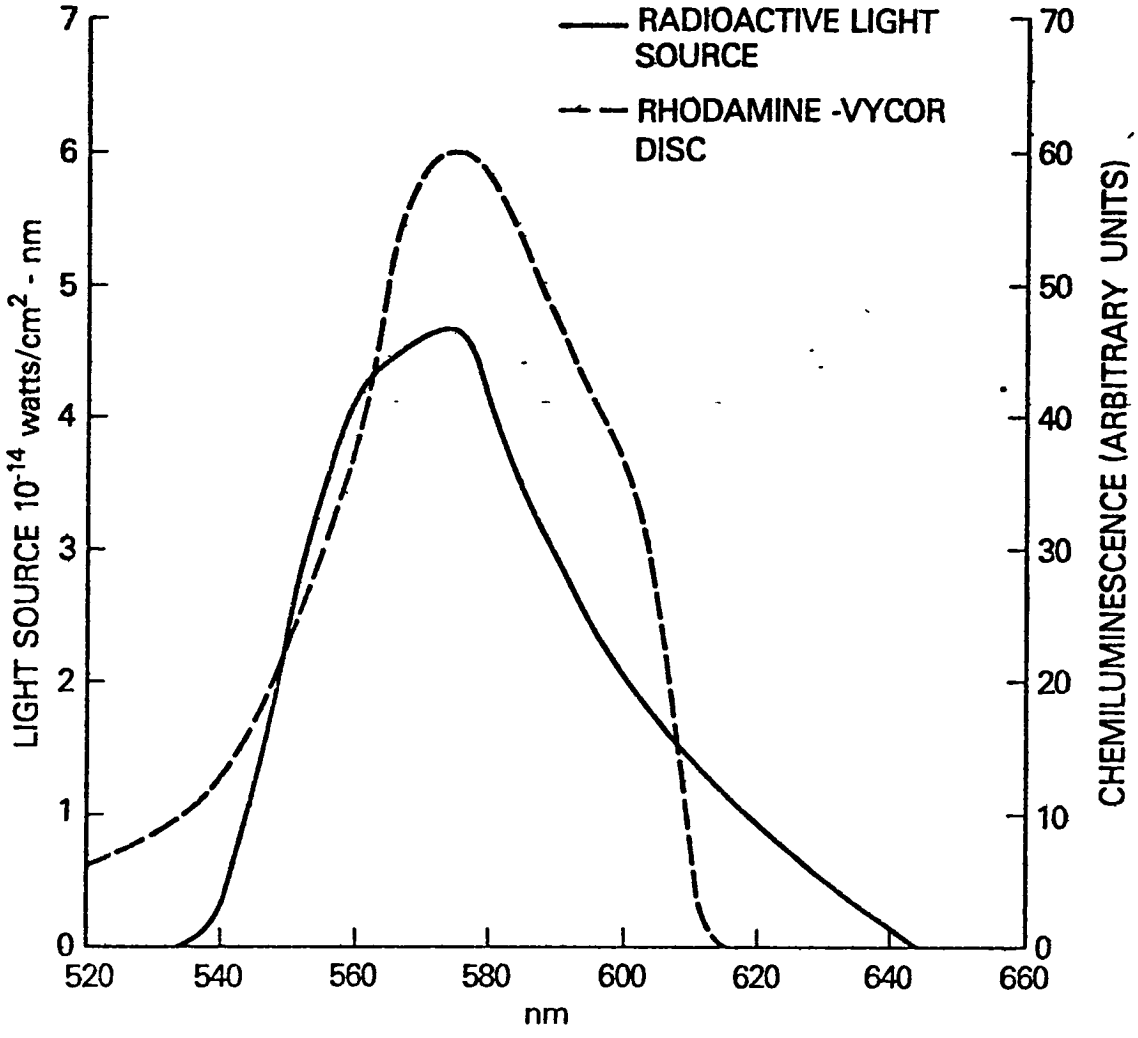

Figure 2. Chemiluminescence spectrum from Rhodamine-Vycor disc excited by ozone and spectral distribution of light source-filter combinations

overcome by removing the contaminating constituent. Laboratory studies have shown a chemiluminescent response to atomic oxygen (the concentration of ozone and atomic oxygen is equal within an order of magnitude at 60 km). Fortunately, oxygen atoms are highly reactive and, hence, easily removed. The sensor inlet pipe as shown in Figure 1 is designed (material and length) to remove all traces of atomic oxygen. This has been demonstrated in the laboratory under extreme conditions of flow and atomic oxygen concentration. Interference of other constituents have been summarized by Hodgeson, et. al. (17). They indicate that NO_2, SO_2, peroxyacetal nitrate, H_2O_2 peracetic acid, H_2S, propane, H_2O, NH_3, NO, and Cl_2 yielded no chemiluminescence, nor did they decrease the sensitivity of the reactive surface to ozone. It is known, however, that water vapor and possibly ammonia give a temporary enhanced sensitivity to the chemiluminescent material. For this reason, the chemiluminescent material and ozone detector volume are kept in a dry and controlled environment during storage, calibration, and payload preparation.

The effect of temperature has been determined by Seiden (18), who found a temperature coefficient to be about a two percent change in sensitivity per degree increase in temperature, near room temperature. The detector cell temperature is monitored during calibrations and flight to account for temperature sensitivity.

3. Chemiluminescent Disc Preparation

The detailed procedure for the preparation of the chemiluminescent disc is given in Appendix A and is summarized below. Porous Vycor, a form of borosilicate glass, is etched in heated NaOH after being cut into 25 mm diameter and 5 mm thick dics. Once the discs are etched and dried, they are dipped in an acetone solution of rhodamine-B dye and gallic acid. The addition of gallic acid ($C_7H_8O_6$) is after a suggestion of Bersis and Vassiliou (19) who found increased stability of the chemiluminescence with this reagent. They found that gallic acid in a solution of rhodamine-B in ethanol is an efficient reducing agent for ozone and that the energy liberated is

transferred to the rhodamine-B, resulting in the luminescence. The gallic acid oxidation is more efficient and faster than rhodamine-B alone, resulting in greater quantum yield, but still protecting the rhodamine-B, thus yielding greater stability. The impregnated discs are cooled, neutralized, and dried. In order to stabilize a disc, it is exposed to high amounts of ozone for several minutes. After this exposure, the disc is exposed to ozone only in amounts produced during the calibration procedures. This will be discussed in more detail in the section on calibration.

4. Response Time

Measurements of chemiluminescent response time at flight conditions are difficult to perform since they would require a means of stepping ozone concentration at low flow rates and reduced pressure. Experiments using the calibration apparatus, discussed in Section IV, indicate that response time is limited by the rate that ozone concentrations can be altered in the laboratory.

The response of the chemiluminescence depends on several factors: 1) The reaction mechanism described in section 1, 2) flow rate, 3) pressure and 4) condition of the chemiluminescent surface with regard to contaminants, moisture, prior exposure to ozone, and age. From the discussion in section 1, it would seem that the reaction mechanism is quite rapid. Flow rate and pressure dependence will be discussed in the section on air sampling. Laboratory experiments of response time performed by Hodgeson, et. al. (17), at atmospheric pressures using 0.2 ppm ozone indicate high response with some overshoot, and a decay period when the ozone source is removed. They explained the overshoot as activation of the chemiluminescent material which is dependent on the age and condition of the material. However, this characteristic is virtually eliminated by proper disc preparation, low exposure to ozone during calibration, and careful storage The observed decay characteristics are most likely due to diffusion of residual ozone molecules to the reactive material. This is confirmed by recent experiments which

demonstrate that decay signals are pressure dependent and therefore diffusion controlled Residual signals due to diffusion are only significant, however, when mean flow past the detector is very small. Since flow is always maintained during the flight, these signals are not significant.

B. Air Sampling Technique

During flight, ambient air is sampled by self pumping which can be described in the following manner using Figure 1. After the payload is separated from the rocket near flight apogee (75 km), the sonde descends through the atmosphere on a specially designed high altitude parachute. The ballast chamber empties on the upleg portion of the flight and refills through the inlet pipe to maintain pressure equilibrium with the outside atmosphere as the sonde descends. The flow rate past the detector is proportional to the pressure change in the chamber as will be shown below. The chemiluminescence is then proportional to the ozone flux. This relationship has been demonstrated over several years of laboratory experiments, and more than 30 actual flights.

1. Sampling Principle

A general expression for the light emitted by the chemiluminescent reaction can be written as

$$L = K C_o F (1 - e^{-q/F}) \qquad [1]$$

where L = luminescent light level

K = photon production efficiency and instrument calibration constants

C_o = ozone concentration

F = flow rate

q = detector cell efficiency related to geometry and inversely proportional to pressure

At high flow rates, equation [1] becomes

$$L = K C_o q \qquad [2]$$

which says that at high flow rates the luminescence becomes independent of flow rate and is inversely proportional to the pressure. Luminescence at high flow rates was studied by Steinberger, et al (20), and could be a basis for an alternate approach to the measurement. However, q would be fairly complex to characterize since high flow rates at low pressures would have to be achieved in flight and simulated in the laboratory to establish the instrument sensitivity.

At low flow rates, equation [1] reduces to

$$L = K C_o F. \qquad [3]$$

Under this condition, the luminescence is proportional to the ozone concentration and flow rate. It is in this condition that the ozonesonde described here was designed to operate. A direct measure of the air flow through the inlet tube is not feasible at the low pressures and flow rates anticipated in flight. The flow rate can be derived indirectly, however, by a pressure and temperature measurement in the ballast chamber (Figure 1) in the following manner.

Time differentiation of the ideal gas law, $pv = \frac{m}{M} RT$, results in an expression for the mass flow rate, $\frac{dm}{dt}$

$$\frac{dm_b}{dt} = \frac{d}{dt}\left(\frac{p_b V_b M}{RT}\right) = \frac{M V_b}{R T_b}\left(\frac{dp_b}{dt} - p_b \frac{d \ln T_b}{dt}\right) \qquad [4]$$

where m_b = mass of air

p_b = air pressure

T_b = temperature

V_b = ballast chamber volume

R = universal gas constant

and the subscript, b, refers to conditions inside the ballast chamber. The air temperature inside the chamber changes very slowly, therefore, equation [4] reduces to

$$\frac{dm_b}{dt} = \frac{MV_b}{RT_b} \frac{dp_b}{dt} \qquad [5]$$

which expresses the mass flow rate as a pressure change. Using the flow rate in equation [5] in equation [3], the luminescence becomes

$$L = \frac{K'r_3}{T_b} \frac{dp_b}{dt} \qquad [6]$$

where r_3 is the ozone mass mixing ratio. Equation [6] indicates that the ambient ozone mass mixing ratio can be determined by establishing the constant K' (as will be discussed in the section on calibration), and measuring the luminescence and the pressure and temperature inside the ballast volume Converting to ozone density requires independent knowledge of the air density

2 Flow Rates In Flight

Pressure changes and flow rates expected in the ozone sensor during the parachute descent can be calculated by assuming pressure equilibrium between the ballast chamber and the ambient air Differentiation of the hydrostatic equation, $p = p_o e^{-z/H}$ yields

$$dp = -\frac{p}{H} dz \qquad [7]$$

and

$$\frac{dp}{dt} = \frac{p}{H} \frac{dz}{dt} \qquad [8]$$

where H is the atmospheric scale height, z the altitude, and dz/dt the parachute descent rate (upward in positive)

Equation [8] can be substituted into [5] to give expected mass flow rates

$$\frac{dm_b}{dt} = \frac{MV_b}{RT_b} \frac{p}{H} \frac{dz}{dt} \qquad [9]$$

while volume flow can be calculated from

$$\frac{dV}{dt} = \frac{RT_a}{Mp} \frac{dm}{dt} \qquad [10]$$

where T_a is the external temperature.

Table I lists the expected pressure change, mass, and volume flow rates in a standard atmosphere, as a function of altitude, using expected descent rates. The last two columns summarize the flow rates determined from a sample of 11 flights. The next to the last column is the average ratio of the measured flow rates (or pressure change) to the calculated flow rate from equation [8]. The table shows that this value approaches unity as the sonde descends. This is expected, since the ballast chamber is not in equilibrium with the ambient pressure at apogee (at 75 km the pressure is 0.02 mb). Therefore, the flow rate must be measured, and not calculated, to remove a possible bias due to residual air in the ballast chamber. The last column is the percent deviation of the ratios, which demonstrates the need for a flow rate measurement on each flight. Altitude resolutions, shown in Table 1, will be discussed in the error analysis section.

One final consideration regarding the air sampling technique is that the chemiluminescence detected at a given altitude is not representative of the ozone concentration at that altitude because the sampled ambient air requires a finite time to reach the detector via the inlet tube. The resultant altitude lag δ_z can easily be calculated from

$$\delta_z = V_c \frac{1}{\frac{dV}{dt}} \frac{dz}{dt} \qquad [11]$$

where V_c is the inlet tube volume and the remaining terms are given in Table I. The volume flow rate and the descent rate both decrease with altitude, therefore, δ_z remains nearly constant at about 0.5 km.

Table 1. Flow Rates for Chemiluminescent Ozonesonde

Mass flow rate $\frac{dm}{dt} = \frac{MV}{R}\frac{1}{T}\frac{dp}{dt}$

Volume flow rate $\frac{dV}{dt} = \frac{R}{M}\frac{T}{P}\frac{dm}{dt}$

Pressure change $\frac{dp}{dt} = \frac{dp}{dz}\frac{dz}{dt} = \frac{P}{H}\frac{dz}{dt}$

Altitude z (km)	Descent Rate dz/dt (m/sec)	Pressure Change dp/dt (torr/sec)	Mass Flow Rate dm/dt (gm/sec)	Altitude Resolution Δz (km)	Vol. Flow Rate dv/dt (cm^3/sec)	Press. Change Ratio* (meas /calc)	Percent* Deviation
70	225	1 3 -3	2 4 –6	4.20	29	.54	70
65	190	2 2	3 8	2.10	23	49	43
60	130	2 9	4.7	1.10	15	.66	19
55	90	3 6	5.6	0.61	9 8	.81	15
50	65	4 8	7 1	0.34	6.9	.88	12
45	45	6 4	9 7	0 18	4.9	93	13
40	30	9 4	1.5 –5	0.08	3 7	.95	10
35	25	1.5 –2	2 5	0.04	2.9	.97	7
30	20	2.2	3.9	0 02	2.1	–	–
25	10	3 5	6 3	0 01	1 6	–	–

*Compiled from 11 Soundings

III INSTRUMENTATION

The ozonesonde has a cylindrical shape, 10.5 cm in diameter and 51 cm long and it is shown in Figure 3. It weighs approximately 2.4 kg including flight batteries and telemetry package. The batteries contain sufficient power to operate the sensor for 50 minutes, which is an adequate time to complete a mission.

To minimize the weight of the sensor, much of the structure also defines the flow path that the sampled atmosphere must travel All surfaces, which are in contact with the air sample, have either been anodized using a special procedure, or they are fabricated from stainless steel Laboratory investigations have shown that the anodization provides a superior, ozone-inert coating which can be cleaned effectively and which does not destroy ozone. The anodization procedure is detailed in Appendix B

The air inlet tube (Figure 1) is 30 cm long and is sufficient to eliminate atomic oxygen present in the ambient air as described earlier. The sampled air then traverses a light trap which consists of several right-angle turns totaling 360 degrees, to prevent sunlight from reaching the photomultiplier tube. The air then enters a chamber where the ozone detector is located. The ozone detector is removable through an access port, should this become necessary. From this chamber the air mixture passes through a transfer tube to the ballast tank

The chemiluminescence is measured by the photomultiplier tube through a glass window. A shutter, edge-driven by a miniature D C motor, interrupts the signal obtained from the detector yielding a pseudo-alternating signal This signal is then amplified by the photometer amplifer yielding a "high" and "low" sensitivity output, both of which are telemetered. The "high" output is ten times greater than the "low "

The ozone detector is a glass disc, 25 mm in diameter and approximately 2 5 mm thick, onto which rhodamine-B has been adsorbed The glass is chemically 96 percent silica ($Si\,O_2$)

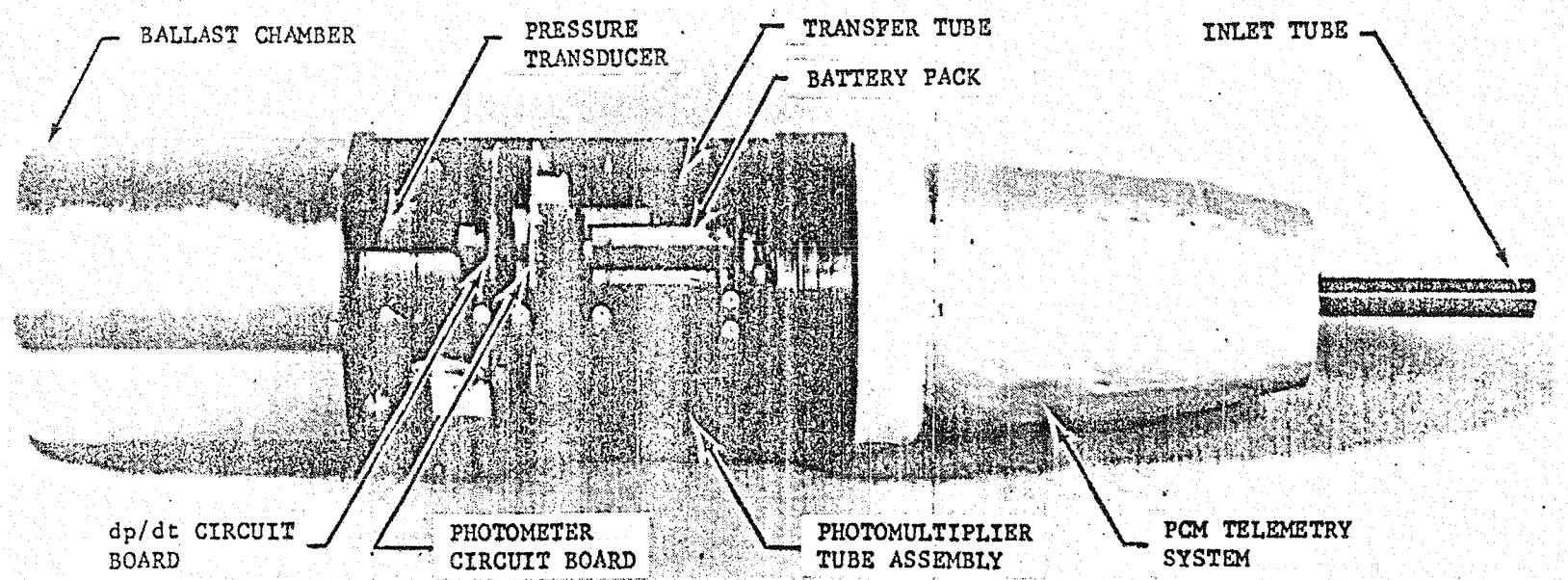

Figure 3. Ozonesonde

and 4 percent boric oxide and is manufactured by Corning Glass as Vycor® 7930. It is porous and, therefore, an excellent adsorbing material. The pore size is typically 40 angstroms, and the available surface area is 200 m^2 per gram of glass The current recipe for the preparation of the chemiluminescent material is described in Appendix A.

The photometer consists of an RCA 8644 photomultiplier tube and is powered by a Venus Q-15 high voltage power supply. The photomultiplier tube which has an S-20 response is especially selected for low dark current noise and high sensitivity. Both are installed in a pressure-tight housing in a dry nitrogen environment to prevent high voltage discharges (corona) from occurring when the ozone sensor is subjected to low atmospheric pressure during flight. A calibration lamp, consisting of a light emitting diode (LED), is activated every 105 seconds for 5 seconds. The LED is detected by the photomultiplier and therefore monitors the performance of the photometer In addition, the power source to the high voltage power supply is also monitored to measure the stability of the photometer.

The pressure inside the ballast tank is measured by a diaphragm type, variable reluctance, absolute pressure gauge. The gauge, a Validyne AP-78, has a range of 0 – 5 torr. The output of this gauge is processed electronically to yield the pressure derivative with respect to time, dp/dt, during the descent of the sensor Both the pressure and dp/dt measurements are telemetered to the ground receiving station A thermistor is mounted on the ballast tank bulkhead to indicate the temperature of the air in the ballast chamber This output is also telemetered to the ground receiving station

The ozone payload shown in Figure 4 is carried aloft on a Super Arcas rocket motor. The Super Arcas, manufactured by Atlantic Research Corporation, is 11.5 cm in diameter and 192.5 cm long and is capable of carrying a 6 kg payload to an altitude of 75 km, when launched at an

® Name registered by Corning Glass Corning New York

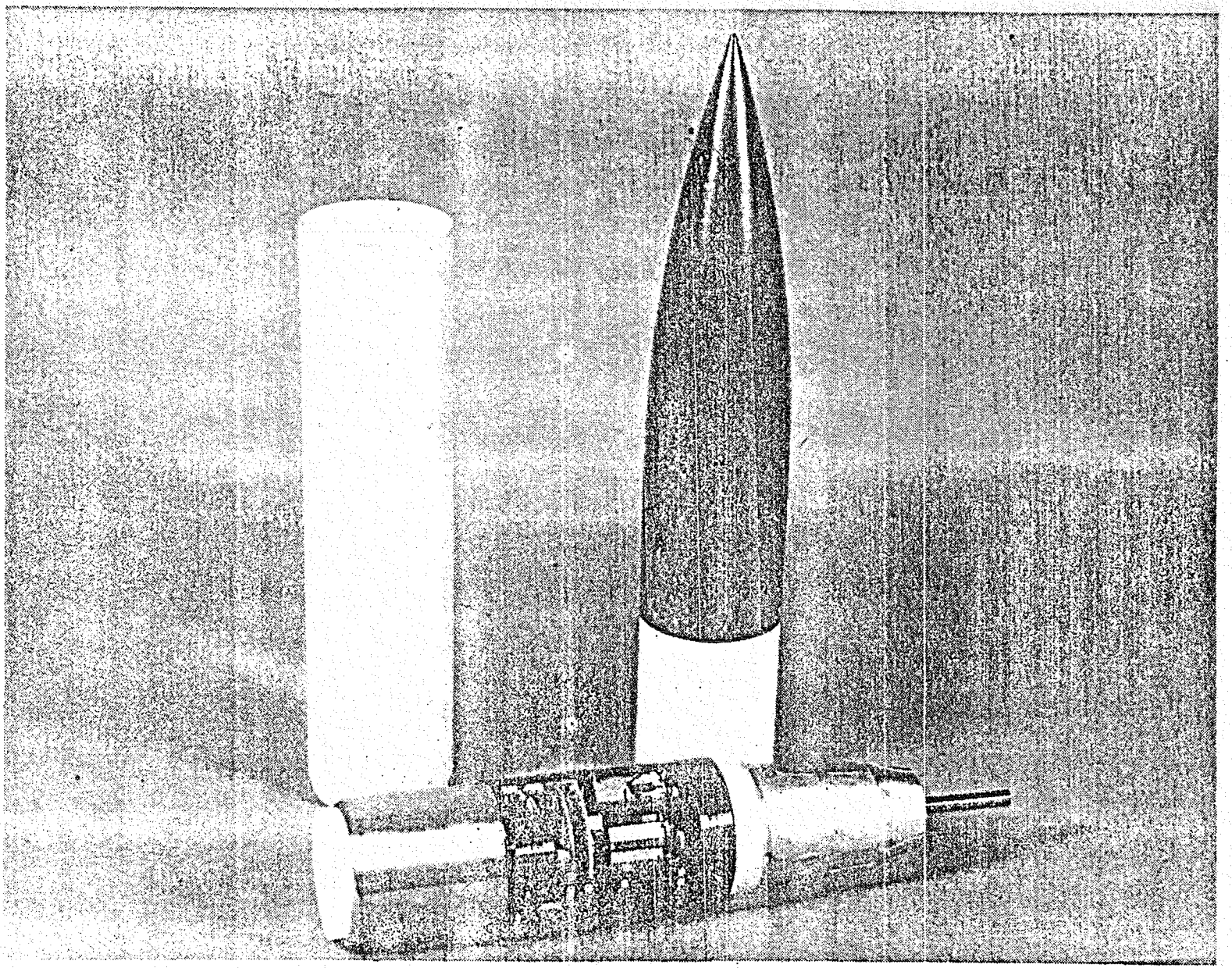

Figure 4. The ozone payload consisting of the sonde, parachute housing, and nose cone

elevation angle of 84 degrees The motor weights 38 kg which makes it possible for two persons to handle it during pre-launch activities without the aid of mechanical handling equipment. This feature is particularly attractive when launches are conducted at temporary launch sites at remote locations.

During ascent, the ozonesonde, including the descent parachute, is packaged inside an aluminur cylindrical housing topped by an asbestos phenolic nose cone (Figure 4). The cylindrical housing also contains a piston which, during the ejection sequence, separates the nose cone and pushes the ozone sensor with attached parachute out of the housing The piston travel is limited to the length of the payload housing by restraint cables and all the gaseous products of the expulsion charge are trapped thereby preventing contamination of the immediate atmosphere. The expulsion charge, a part of the rocket motor, is a pyrotechnic device initiated at burnout of the rocket motor It is pyrotechnically delayed to 146 seconds after launch and causes the ozonesonde to be ejected near apogee After ejection, the parachute, now free of its deployment bag, opens and decelerate the ozonesonde all the way to the surface

The ozonesonde signals are telemetered via an 8-channel pulse code modulated telemetry system operating on 1680 MHz carrier frequency The ozone sensor and telemetry system are powered by six Yardney HR 1 5 silver cell batteries This supply powers a DC/DC converter which powers the sonde subsystems The sonde can be powered either externally or internally (by the batteries) from a payload control box The sonde telemetry signal is recorded by a standard GMD meteorological ground station prior to launch during the upleg portion of the flight and during the descent to about 20 km Additional details of the telemetry system and sensor interface are given in Appendix C

IV CALIBRATION

The chemiluminescent ozone measurement is not absolute, therefore, the ozone sensor requires preflight calibration to determine its sensitivity to ozone. From equation [6] the ozone mixing ratio, r_3, is derived from

$$r_3 = \frac{T_m}{K'} \quad \frac{L_m}{(dp/dt)_m} \qquad [12]$$

where the subscript, m, refers to the flight measurements and K', the calibration constant. K' is determined from laboratory measurements of luminescence as a function of the ozone concentrations, pressures, and flow rates expected in flight The simulation-calibration apparatus is depicted schematically in Figure 5 and photographically in Figure 6. The calibration is performed by evacuating the entire apparatus with the ozone sensor attached and allowing it to refill with a known ozone and air mixture at the rates expected in flight These rates are derived from equation [8] and are listed in Table I

The ozone sensor calibrator is largely a glass apparatus consisting of a 22 liter sphere, a number of high vacuum stopcocks and a variable Teflon leak valve. Glass has been found to be easily cleanable and nonreacting with ozone An absolute pressure gauge measures the pressure inside the glass sphere and the ozone sensor and serves as a check for the performance of the sensor's pressure gauge Ozone for passivation is generated by the high concentration generator, whereas for calibrations, the low concentration generator is used Both operate by exposing air or oxygen flow to the 254 nanometer emission line from a low pressure mercury lamp. During calibrations, the flow is continuously measured by a Dasibi Ozone Monitor The ozone monitor is highly stable and is calibrated against a UV photometer at the National Bureau of Standards The flowmeter is used to verify that sufficient gas flow is present in the system, because the ozone monitor requires a flow of 3 liters per minute to operate accurately. Only a small percentage of the total available flow actually enters the glass sphere and the sensor during

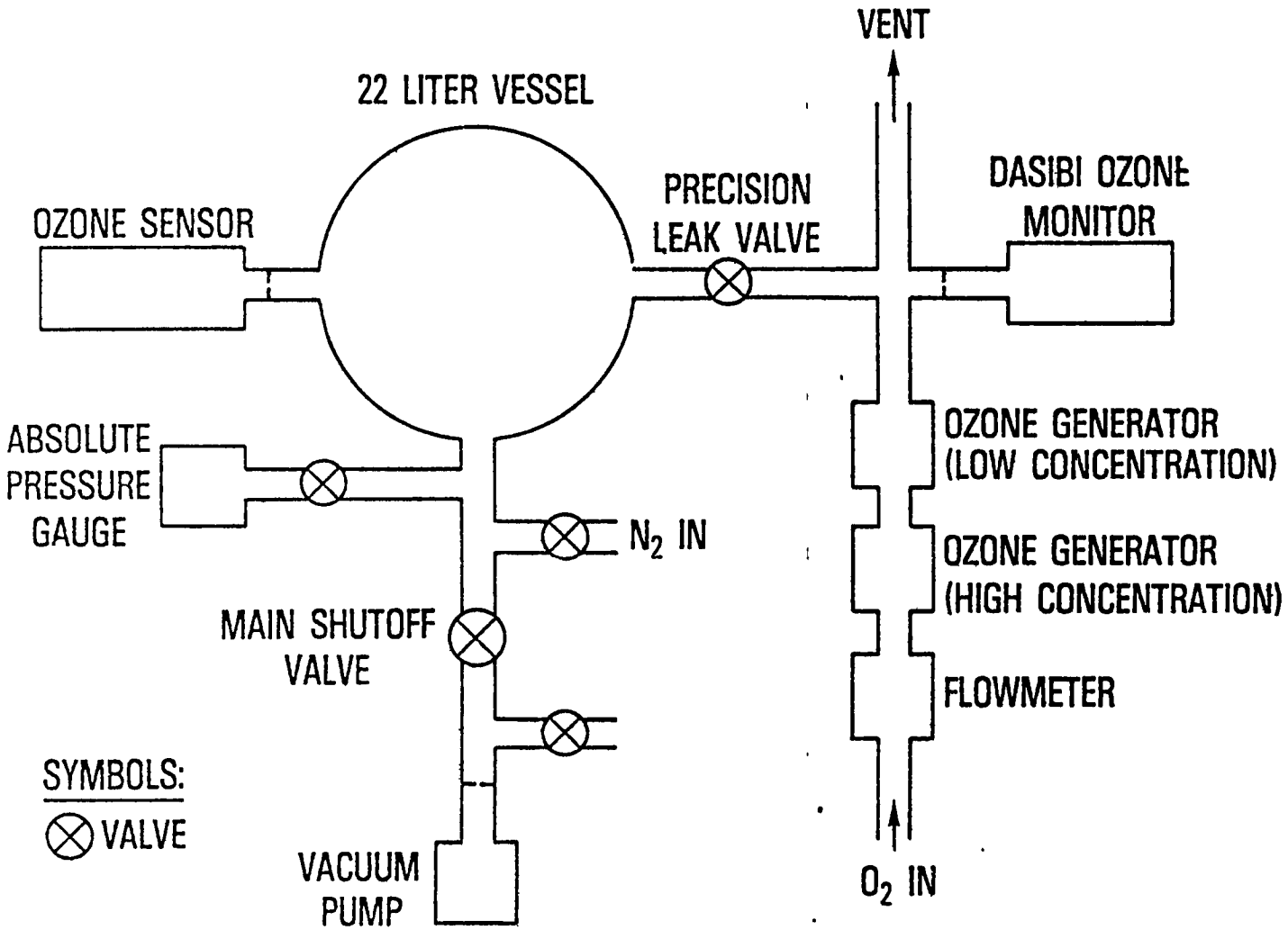

Figure 5. Block diagram of ozone sensor simulation-calibration apparatus

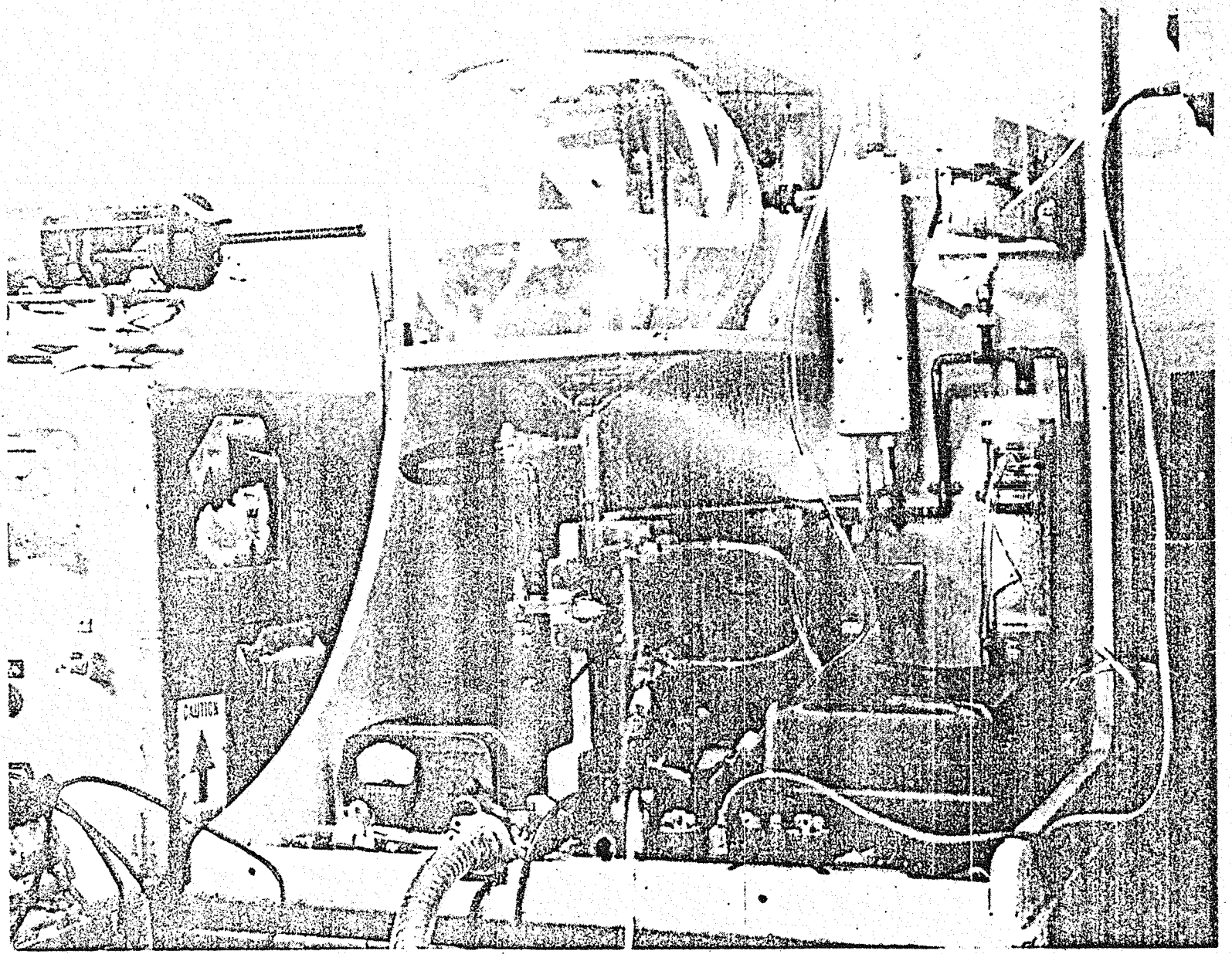

Figure 6. Photograph of ozone sensor simulation-calibration apparatus. Ozone sensor is seen at left and a portion of the Dasibi ozone monitor is seen in upper right corner

calibrations through the variable leak valve. A vacuum pump capable of evacuating the sphere and the sensor to a pressure of less than 0.1 torr is part of the calibrator.

Prior to calibration, the ozone sensor must first be passivated. Passivation is a preconditioning procedure, whereby the calibrator and ozone sensor are exposed to flow of oxygen containing a high concentration of ozone (concentration > 100 PPM of O_3). Any potential ozone-destroying substance present is eliminated by this procedure and is extremely important if low ozone concentration measurements are to be successfully performed. A typical calibration procedure follows a repeating pattern. A sensor may be passivated only every few days; however, the calibrator is passivated every day. The ozone detector is always removed from the sensor during passivation, because the detector would be totally destroyed if exposed to the high ozone concentrations for a lengthy period of time After passivation, which lasts from 12 to 24 hours, the sensor and calibrator are pumped out a few times and flushed with pure nitrogen gas to remove all ozone. The ozone detector is then installed, and the sensor and calibrator are evacuated to less than 100 millitorr. Ozone at a known concentration is introduced into the sensor at leak rates from 4 to 16 millitorr per second in steps of 2 or 4 millitorr per second at approximately one minute intervals. During these intervals the pressure rises from 100 millitorr to about 5 torr. The leak rates (or flow rates), obtained from the sensor's dp/dt channel, and the luminescence, yielded by the "high" or "low" sensitivity channels, are recorded on a paper strip chart recorder. Plots of the luminescense versus dp/dt at several ozone mixing ratios yields the calibration constant, K', from equation [6] For a new, never-used ozone detector, a linear relation is seldom obtained right away, nor is a stable value of K' determined Stability and linearity are achieved by the time 20 calibrations have been performed.

Once this stability has been reached, the sensor is stored with the chemiluminescent detector and filled with dry nitrogen Sensitivity is checked once or twice a day in preparation for flight to assure that no change in calibration has occurred. Occasionally the sensor might require

additional passivation and will then require additional calibration These procedures are most critical in the performance of this experiment. Careful sensor preparation and calibration will result in a highly linear response and calibration stability to about 5 percent. The uncertainty of the calibration to the overall accuracy of the experiment is discussed further in the Error Analysis Section below.

V. ERROR ANALYSIS

In order to perform meaningful satellite comparisons, the accuracies of the rocket measurement should be comparable to or better than the satellite measurement. The stated accuracies of the satellite sounders are in the range of 5 – 20 percent. In addition, rocket experiments for geophysical research should have high precision. Diurnal changes below 50 km are expected to be small, whereas in the region of 70 km, they could be a factor of two. Short term changes in the upper stratosphere are probably of the order of 10 – 20 percent. These changes, then, provide some perspective to the required accuracy and precision for satellite comparisons and geophysical experiments.

For the purpose of this discussion, the experimental errors are classified into three categories. 1) Independent random errors within a given flight; 2) Systematic errors that bias the measured ozone profiles from one flight to the next; and 3) Experiment bias errors which involve the absolute accuracy of the measurement technique These are discussed separately below and are then combined to give the estimated precision and absolute accuracy of the measurement.

A. Random Flight Errors

Above 60 km, random errors unique to a particular flight are in large part associated with instrumentation low signal-to-noise ratio and short integration times. In this altitude range, chemiluminescent light levels and pressure gauge response are low, and signal-to-noise ratios range from one to ten Moreover, the flight data are noisy, because of rapid oscillations of the sonde just after the payload separates from the vehicle. Pressure gauge noise, due to high inertial forces on the pressure gauge diaphragm, results in unintelligible changes in flow rate data The payload oscillations continue until sufficient drag stabilizes the parachute

The sonde descends approximately 5 to 10 km (from 75 km) during the stabilization period Typically, the RMS errors from the pressure gauge and photometer are 20 – 30 percent between

70 and 60 km These errors decrease rapidly and approach about 2 percent below 60 km where the sensor signals become large and the descending sonde is highly stable. Telemetry resolution and altitude accuracy is of the order of one-half percent

The above errors are combined in the following manner to yield an estimated random flight error, E_R

$$E_R^2 = E_A^2 + E_t^2(P) + E_t^2(F) + E_f^2(P) + E_f^2(F) \qquad [13]$$

where the subscripts A, t, and f refer to errors in altitude, due to telemetry noise and, as a result of the flight environment, respectively. E(P) and E(F) are errors in the photometer and the flow rate measurement, respectively. Using equation [13] and the values given above the random flight errors, E_R starts out typically at 35% from apogee (75 km) to about 60 km, then very rapidly decreases to about 5% below 60 km. E_R varies from flight to flight but can be computed.

B Systematic Errors for a Given Sounding

Systematic errors combined with random errors influence the precision of the experiment and could result in biases between flights. These errors can be instrumental in origin or due to uncertainties in the calibration Large instrument errors are unlikely, once the calibration procedures are completed. Photometric stability is assured by the high voltage monitor and the onboard light source. However, for this analysis, it is assumed that a 2 percent change in photometer sensitivity could go undetected Absolute accuracy of the pressure gauge is not required, since the sensitivity of the gauge is included in calibration constants. Errors could arise, however from shifts in the gauge linearity or sensitivity, but would be limited to 2 percent

The largest source of systematic error is the uncertainty in the calibration constant, K′, in equations [6] or [12]. Each ozone sensor is calibrated prior to the flight, therefore, an error in K′ can be associated with each sounding. The error in K′ includes uncertainty in repeatability and linearity in the chemiluminescent reaction as well as the laboratory flow rate and ozone concentration settings and readings. The K′ error can then be evaluated by repeated calibrations using varying flow rates and ozone concentrations. Numerous laboratory experiments and simulations indicate a typical standard error of about 5 percent in K′, though lower values are achievable. This value depends in part on the particular ozone sensor and the number of calibrations performed since the chemiluminescent sensitivity tends to stabilize with time.

Since the above errors are independent, the combined systematic error, E_S, can be estimated by

$$E_s = \sqrt{E^2 (K') + E_c^2 (P) + E_c^2 (F)} = 7.6 \text{ percent.} \qquad [14]$$

where the subscript, c, refers to the calibration measurements.

Now, equations [13] and [14] are combined to give an estimated precision of the measurement, P

$$P = \sqrt{E_R^2 + E_S^2} = 8.1 \text{ percent} \qquad [15]$$

The precision is poorer above 60 km, but is highly dependent on the sonde descent conditions discussed earlier. The precision also varies from flight to flight, depending on instrument noise, tracking data quality, and the uncertainty in the calibration constant.

Comparison of two soundings conducted nearly simultaneously provide a great deal of credibility to this analysis. In a repeatability test, the first sounding was conducted on 24 July 1977 at 04 02 Z (23.02 Local Time) and the second, 13 minutes later. The measured ozone profiles are shown in Figure 7 as ozone mixing ratio as a function of altitude where the soundings are numbered

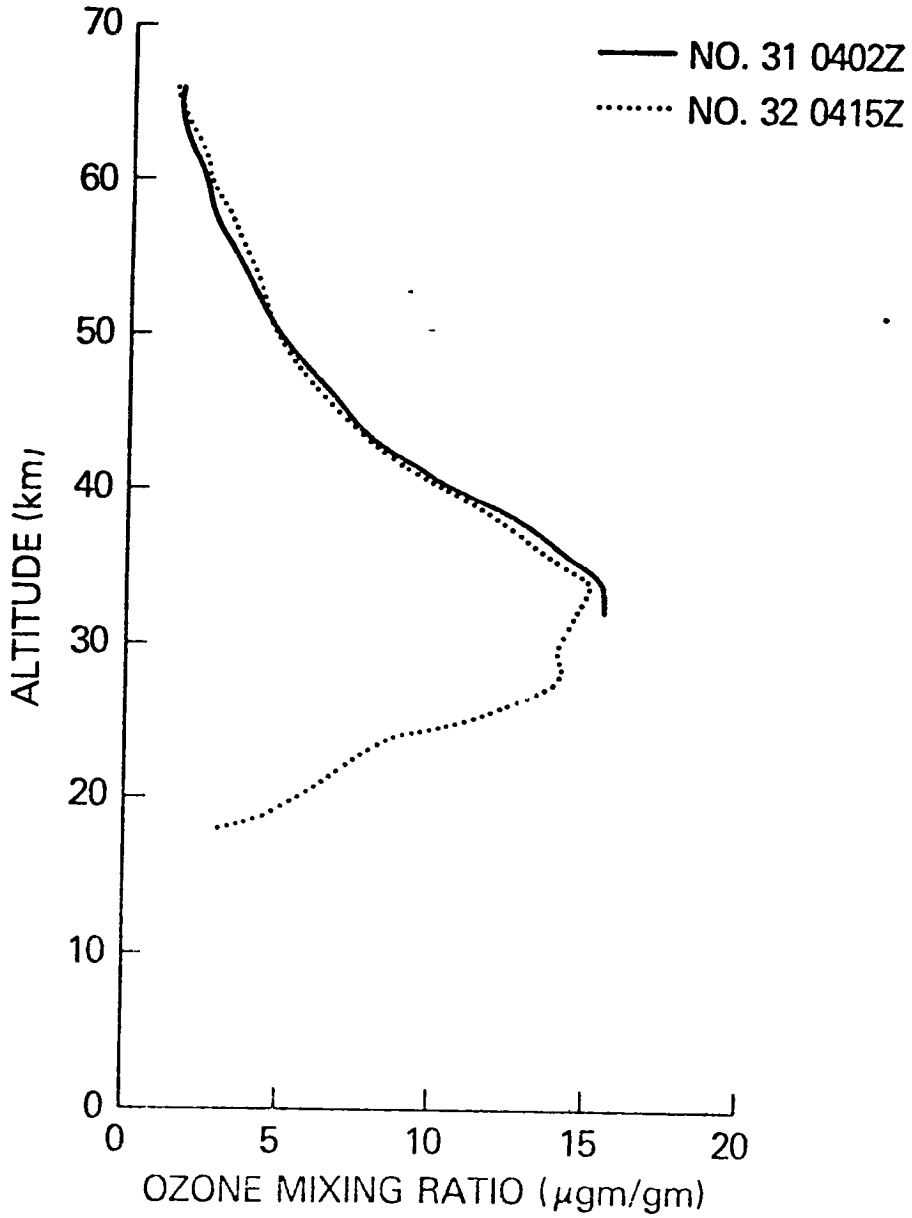

Figure 7 Two ozone profiles measured 13 minutes apart in a repeatability test at Wallops Island, VA on July 24, 1977

31 and 32. No data were obtained from flight 31 below 32 km because of an abrupt instrument failure. The difference from the mean profile between 65 and 32 km is 6.1 percent. This average error was calculated by

$$\frac{1}{33} \sum_{i=32}^{65} \left(\frac{2 \, | r_i (31) - r_i (32) |}{r_i (31) + r_i (32)} \right) = (6.1 \pm 3.6) \text{ percent} \qquad [16]$$

where r_1 is the measured ozone amounts from the two flights at 1 kilometer intervals. This compares very well with the estimated precision of 8 1 percent computed from equation 15.

C. Absolute Errors

Absolute experimental errors are systematic errors that appear uniformly in all the measurements and result in a bias on the average from the real amounts. These errors are most difficult to assess. Examples are: departure from linearity of the chemiluminescence still unaccounted for in the calibration, contamination of the sonde; errors in the absorption coefficient used in the ozone calibration source, and altitude resolution Altitude resolution can be satisfactorily calculated from the measurement principle and is discussed at the end of this section.

The ozone monitor used in the rocket sonde calibration system is well maintained and regularly calibrated at the National Bureau of Standards against an ultraviolet absorption cell which measures ozone by means of absorption at 253 7 nanometers. The error in the true ozone amounts is 3 percent where uncertainties in the absorption coefficient at 253.7 nanometers is the major contributor (A Bass, 1978, Private Communications) The precision in transferring the NBS calibration to the ozone monitor used in the sonde calibration is about 1 percent or less.

An undetected bias may also result from losses of ozone in the sonde calibration system as the air ozone mixture passes through the glass and Teflon valves. Transfer of reactive gases in this manner is common practice and it is reasonable to assume that the ozone mixing ratio

remains constant when the system is well passivated. No ozone losses through the calibration system are detected at atmospheric pressure. If there were losses, the calibrations would result in measured ozone concentrations which are too high. Unaccountable nonlinearities at high ozone concentrations would also result in a high measurement. This error has been detected in balloon comparisons (if balloon sondes are assumed to give true ozone values) below 20 km. Contamination of the ozonesonde prior to flight would be undetected and would result in a measurement that was too low. This error is expected to be small because of careful handling procedures and the payload design which minimizes contamination during flight.

The net absolute error, considering a worst-case condition, can be derived by the following assume that errors due to losses during calibration and unaccounted nonlinearity errors are each 5 percent and additive, while the contamination error is 5 percent, but with the opposite sign The amount by which these errors cancel each other is unknown and, therefore, they are added in the following manner to yield the absolute error, E_A

$$E_A = \sqrt{(5\% + 5\%)^2 + 5\%^2 + 4\%^2} = 11.9\% \qquad [17]$$

where the last term is the error associated with the ozone standard and appears under the square root because it is independent of the other three errors

As mentioned above, absolute experimental errors are difficult to establish and are only estimated for worst case conditions Comparison with other measurements of ozone can provide some insight as to possible errors, however, especially if the other measurement utilizes a different experimental technique. Comparisons have been performed with balloon sondes using electrochemical techniques, however, the altitude region where the measurements overlap is small and a systematic error has been detected Generally, the ozone values measured by the rocket sonde are higher

On two occasions, the chemiluminescent sonde was compared with the Krueger rocket optical sonde (2). On one of these occasions, there was a nearly coincident satellite sounding. The first rocket intercomparison took place in September 1968 and was reported by Hilsenrath, et. al. (4). The comparison illustrated in Figure 8, shows two ozone mixing ratio profiles measured 12 minutes apart, one from the chemiluminescent sonde and the other from the optical sonde. Both experiments measure the mixing ratio peak at 35 km. Above this peak, the differences are about 10 percent with the chemiluminescent sonde showing lower values. Below

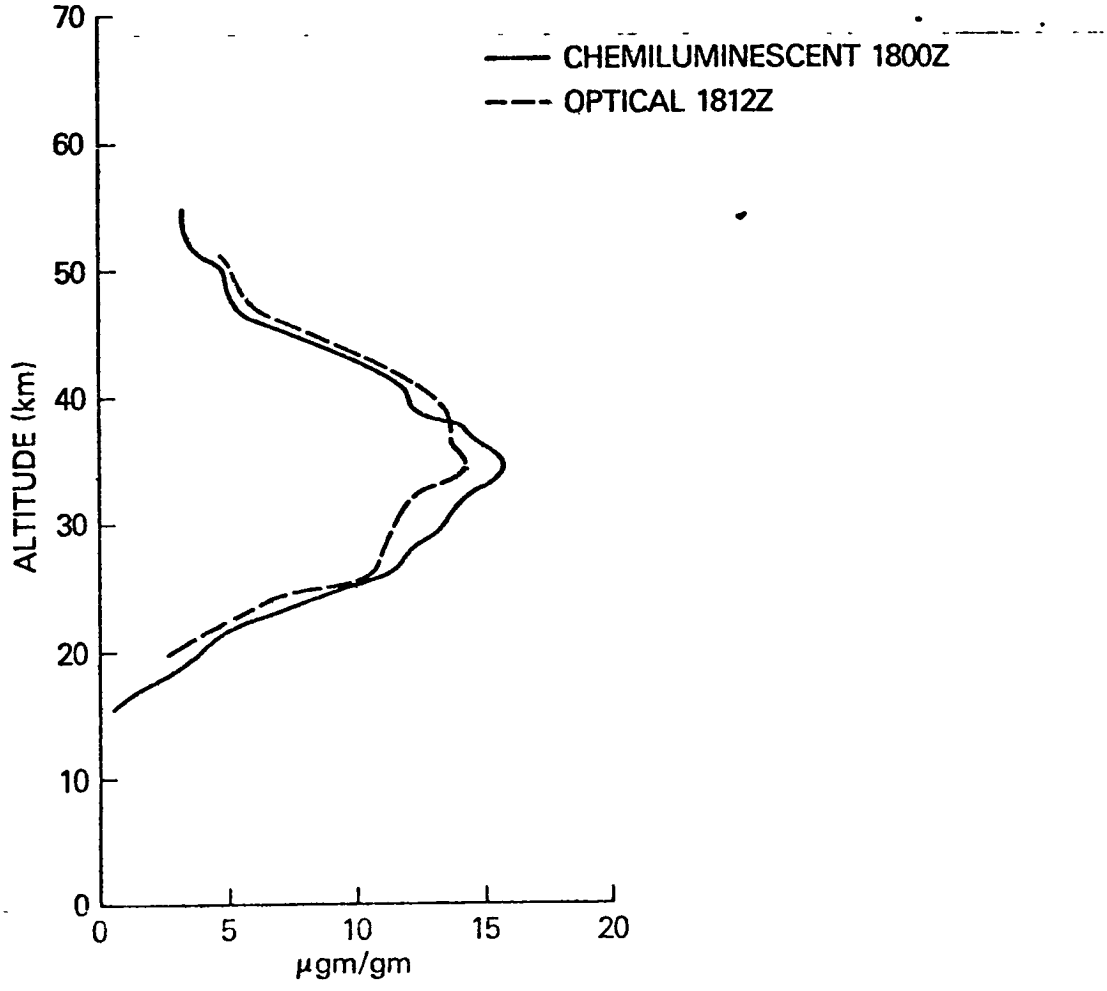

Figure 8. Comparison of ozone profiles measured from chemiluminescent and optical ozonesondes performed at Wallops Island, VA on September 16, 1968

the peak, the differences are about the same however opposite in sign. The comparison was repeated over Wallops Island, Virginia in July 1975, at the time of a Nimbus-6 satellite Limb Radiance Infrared Radiometer (LRIR) overpass which also measured ozone. The rocket and satellite data are shown in Figure 9, which is reproduced from Hudson (21). The agreement between the rocket sondes is good again, however, the differences should be noted. The chemiluminescent measurement is again lower and higher, above and below the mixing ratio peak respectively, than the optical sonde This may represent a real systematic difference between the two techniques. The nearly 20 percent difference at the mixing ratio peak is unexpectedly large but could be due to a time variability, since the rocket soundings were nearly two hours apart.

With regard to altitude accuracy, the position of the payload is known to better than one percent (± 250 meters at 50 km) from a good radar track. Altitude error was considered in equation [13] in estimating random flight errors Altitude resolution, however, involves an experimental limitation and hence affects the absolute accuracy of the measurement. The minimum altitude resolution is defined as the altitude range within which a pressure change (or flow) can be detected. From the earlier discussion of expected flow, differentiation of the hydrostatic equation yielded

$$dp = \frac{p}{H} dz \qquad [7]$$

The altitude resolution, Δz, is then defined as

$$\Delta z = \frac{\Delta p}{p} H \qquad [18]$$

where Δp is the minimum detectable pressure change from the ozone sensor pressure gauge which is about 0.5% full scale or 25×10^{-3} torr Using this value, the solution to equation [18] in 5 km increments is given in the fifth column of Table 1. Above 60 km, altitude resolution is greater than 1 km, while below this level it becomes increasingly finer At 30 km, the altitude resolution is about 20 meters.

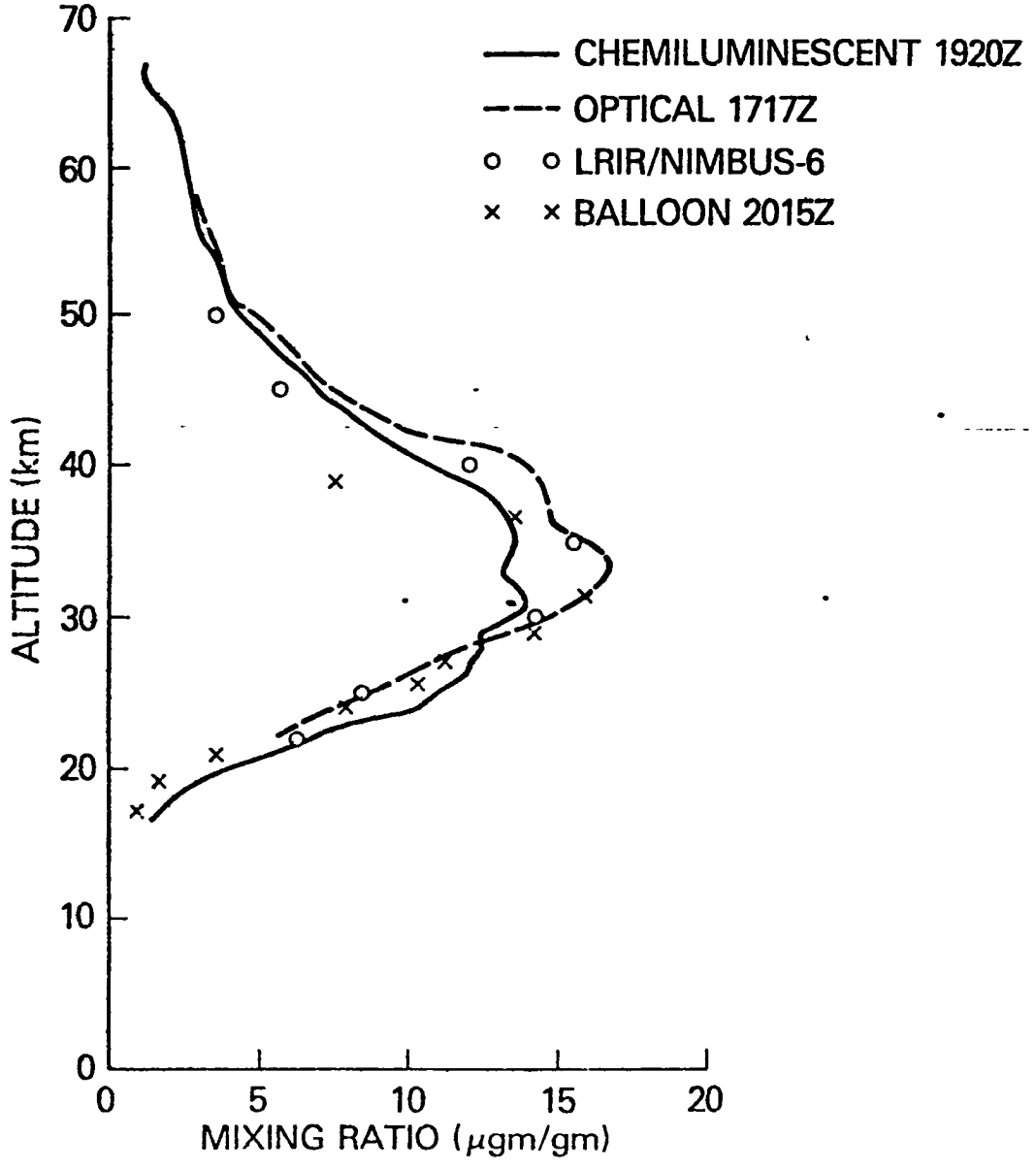

Figure 9. Comparison of ozone profiles measured from 2 rocket sondes, 1 balloon sonde and a coincident Nimbus 6 LRIR sounding on July 29, 1975

Summarizing the error analysis, it was found that random experimental errors are small below 60 km. The precision of a given sounding is highly dependent on the calibration, and can be predicted A sample calculation showed a precision of about 8 percent, and a repeatability test showed a difference of 6 percent between two soundings conducted nearly simultaneously. Absolute errors are difficult to determine, since some error sources tend to cancel each other out, while others are unmeasurable. A worst case calculation showed an absolute error of about 12 percent. Comparison with another rocket measurement using a different measurement principle on two occations showed differences no greater than 20 percent where the average difference was less than 10 percent. Finally, by combining the precision, P and the absolute error, E_A, an estimate of how far a single measurement might be from the true ozone amount may be calculated by

$$\sqrt{P^2 + E_A^2} = \text{measurement error} \qquad [19]$$

since P and E_A are independent. Using a typical value of P equal to 8% from equation [15] and the nominal value of 12% for E_A from equation [17], the combined measurement error is then 14%

VI Discussion of Flight Data

Ozone in the stratosphere and mesosphere has been measured under varying geophysical conditions using chemiluminescent sondes. Some of these experiments are reviewed here and may be used to test various photochemical models. Diurnal variations measured at mid and low latitudes reported by Hilsenrath (22) and by Heath, et. al. (23) show some latitude dependence. In addition, mesospheric and stratospheric ozone were measured during the polar night under a wide range of wind fields and temperatures. The ozone profile variations can, for the most part, be explained by the measured temperature profile variations, however, transport must also be considered even at mesospheric levels. Some of these results were reported by Hilsenrath (22), and new data will be discussed below. In a recent effort to determine the role of the stratosphere in sun/weather relationships, ozone profiles were measured before and after geomagnetic disturbances. The first of these experiments was informally reported by Goldberg and Hilsenrath (24). A second experiment performed in March 1978 showed a similar result; namely, that ozone was significantly depleted above 50 km after a strong auroral event at night Since nighttime or night-to-night changes in the vertical distribution of mesospheric ozone are unknown, these results do not prove the geomagnetic disturbance were responsible for the observed changes.

The measured ozone changes were of the order of 10% to a factor of two in the experiments described above, and in most instances these changes become larger with increasing altitude These changes have been evaluated in terms of the error analysis discussed earlier which does show increasing errors at higher altitudes However, the errors are random and can be evaluated from the flight data Most important is, that the systematic errors or flight to flight biases are not altitude dependent Therefore, ozone profile changes reported here and earlier, except for one to be discussed below are therefore likely real.

A. Daytime Stratospheric and Mesospheric Ozone at Midlatitudes

The first ozone profiles measured over Wallops Island, VA, in September 1968 were reported by Hilsenrath (4) (shown in Figure 8 with data deleted above 55 km) and indicated an increasing mixing ratio above 57 km and a small peak at 62 km. The reported error then was 50% at this level. Reevaluation of the flight data using the error analysis described above resulted in an error of 200% above 57 km, decreasing very rapidly below this level to the values of 20% previously reported. Therefore, the secondary peak (around 60 km) measured in the daytime lower mesosphere is most likely not real. Figure 10 depicts daytime ozone distribution over a single station, Wallops Is., VA, over a seven-year period, and includes the

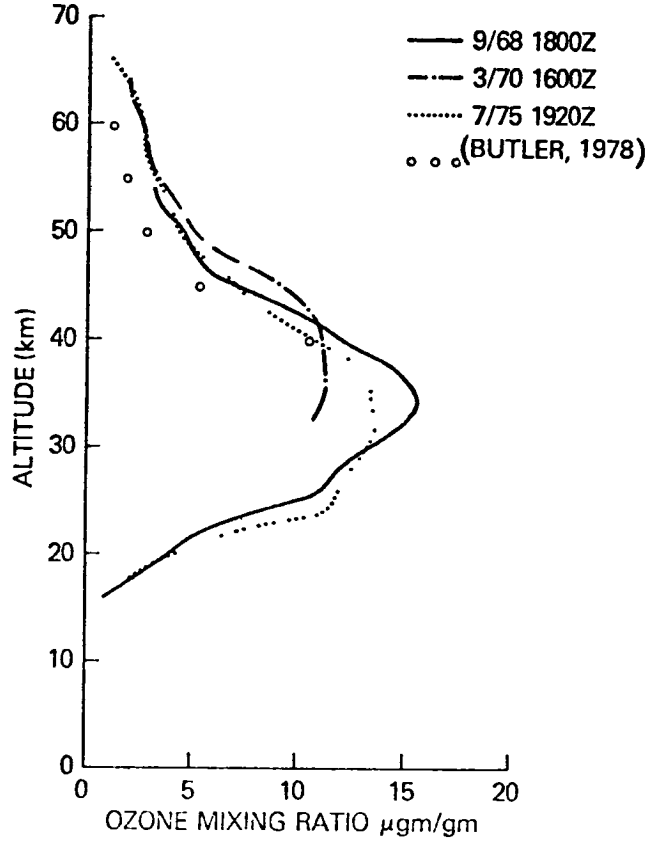

Figure 10 Summary of ozone profiles measured over Wallops Island, VA over a seven-year period compared with one-dimensional photochemical model (27)

September 1978 measurement The combined accuracy, absolute and precision, is about 15% in the altitude range 25 to 60 km for the measurements of March 1970 and July 1975. The differences shown, then, include real seasonal and interannual variability. To some degree, the data show stability in the ozone distribution above 50 km.

The ozone values shown in Figure 10 agree fairly well with the model by Krueger and Minzner (25), as they should since these data are part of the model. However, there are significant discrepancies with the measurements of Watanabe and Tohmatsu (26), who report summer mean values about 40% lower than those shown in Figure 10, and nearly doubling for a winter mean, in the altitude range of 50 to 60 km at a comparable latitude over Japan It should be pointed out, however, that none of the soundings shown in Figure 10 are in winter and that the mean values reported by Watanabe and Tohmatsu consist of three flights for summers ranging from 1966 to 1975, and seven flights in the winters ranging from 1965 to 1975.

This discrepancy has important implications to the validation of photochemical models used in ozone depletion studies, since the altitude range where the rocket measurements disagree has relatively simple chemistry and is least influenced by dynamics. Butler (27) has pointed out an apparent conflict between one dimensional photochemical models used for stratospheric depletion studies and the observations, namely the Krueger and Minzner empirical model (25). Butler's photochemical model calculations for 30° latitude shown in Figure 10 result in values which are about 40% lower than the rocket observations (as well as the Krueger and Minzner model) but comes close to the summer values of Watanabe and Tohmatsu (26) at 50 km Unfortunately the data shown in Figure 10 do not help resolve this dilemma. Uncertainties in HO_x chemistry and unexpectedly large variations in mesospheric water vapor are often used to explain the model discrepancies and the variation in the observations.

B Nighttime Stratospheric and Mesospheric Ozone at Low Latitudes

Nighttime ozone profiles were measured at low latitudes on four occasions. Two flights were conducted in May 1975 at 9S, and two at 5N in March 1971 and March 1975. Three of these flights had larger than the usual random errors and uncertainties in the calibration constants. A composite ozone profile formed by a weighted average of the four profiles is shown in Figure 11. The horizontal bars represent a one sigma estimate for the composite profile.

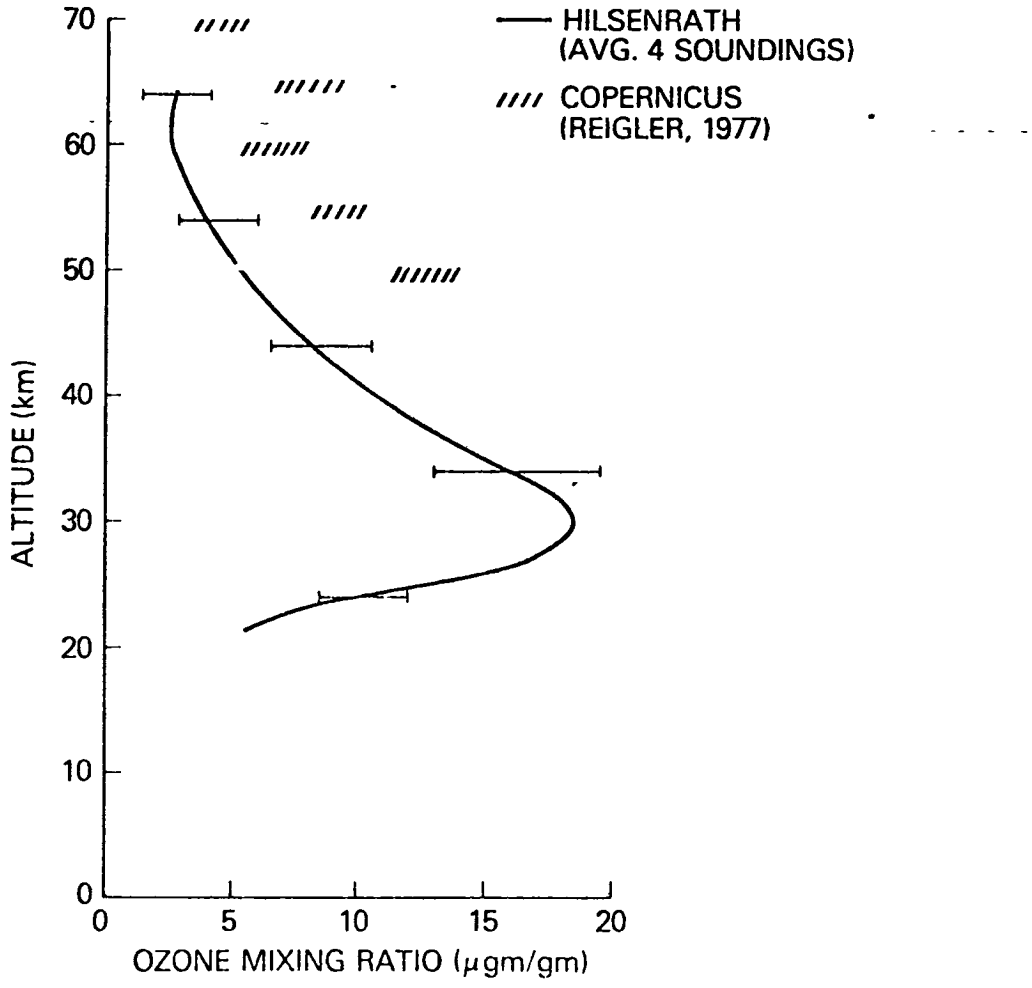

Figure 11 Composite ozone profile derived from four rocket measurements compared with three Copernicus satellite occultation measurements during the equatorial nighttime

These data are compared to nighttime equatorial profiles derived by Riegler, et al. (28) from ultraviolet stellar occultation satellite measurements on three occasions in 1976 (mixing ratios were computed using the 1962 U.S Standard atmosphere for low latitudes). The figure illustrates not only that the average value differ by a factor of two, but also that the ranges from the two measurements do not even overlap.

Radiative equilibrium temperatures were computed by Kuhn et al. (29) for the Krueger and Minzner model (25) and Riegler's (28) stellar occultation ozone profiles and then compared to the temperature profile from the U S. Standard Atmosphere Supplements, 1966 Though Kuhn, et al. (29) confuse the Krueger and Minzner ozone profile with ozone data from the Backscattered Ultraviolet experiment (BUV) in the Nimbus-4 satellite, they show that the calculated temperature profile from the Krueger and Minzner model (25) comes closer to the U.S Standard temperatures above the stratopause than does the profile from the stellar occultation observations (28) at low latitudes. They still conclude, however, because of a number of uncertainties, that the occultation measurements cannot be discounted on energy balance arguments alone

C. Stratospheric and Mesospheric Ozone in the Polar Night

A measurement series was conducted at Pt Barrow, Alaska, and Thule, Greenland, to determine the behavior of the vertical ozone distributions during the polar night. Specifically, the plan was to measure ozone during a stratospheric warming, or before and after the breakdown of the winter polar vortex The earlier flights in Alaska were coordinated with rocket grenade soundings which measured temperature and winds well into the mesosphere A total of 7 soundings of ozone was obtained in the winter and early spring Two of the Greenland flights in December 1975, were also coordinated with LRIR ozone soundings from the Nimbus-6 satellite. Two flights from Alaska in January 1969 were reported by Hilsenrath (22) These soundings showed significant changes in ozone above 50 km, where the ozone

mixing ratio decreased by a factor of two for a 50°C temperature change. Another measurement was performed in Alaska in December 1971 as a baseline measurement prior to a stratospheric warming. No major wintertime disturbance developed after several weeks, and the expedition was abandoned. In May 1972, one flight was made at Pt. Barrow to compare with the Nimbus-4 BUV at high solar zenith angles.

Figure 12 illustrates the ensemble of ozone profiles measured during the arctic winter. Comparison with Figures 10 and 11 shows significant variability at nearly all levels. Ozone mixing ratios vary by 50% from 20 to 45 km and even more above 60 km. Figure 13 illustrates the temperature profiles measured at the same time as the ozone measurements. The large temperature variations seen here in winter high latitudes were shown by Heath, et. al. (23) and are well known. They reflect the large variability of the winter at high latitude upper atmosphere. The expected temperature related changes in ozone of a few percent per degree can only account for some of the observed ozone variations, and a statistical analysis of the ozone and temperature values at all levels revealed only a weak correlation. A most unusual profile was obtained on December 6, 1971, where the ozone mixing ratios above 60 km exceeded that at 40 km. An ozone buildup in this altitude range can be explained by a source of atomic oxygen from much higher altitudes or from lower latitudes. Atomic oxygen from sunlight regions can combine with molecular oxygen enhancing the ozone concentration in the absence of sunlight. The absence of hydroxyl radicals in dark regions of the atmosphere would allow a further ozone buildup above 50 km. However, during extended periods of darkness, photochemical equilibrium should not be expected, since photochemical lifetimes are long and dynamic processes are most intense during the winter months at high latitudes. Horizontal and vertical transports, then must play an important role in explaining the ozone observations.

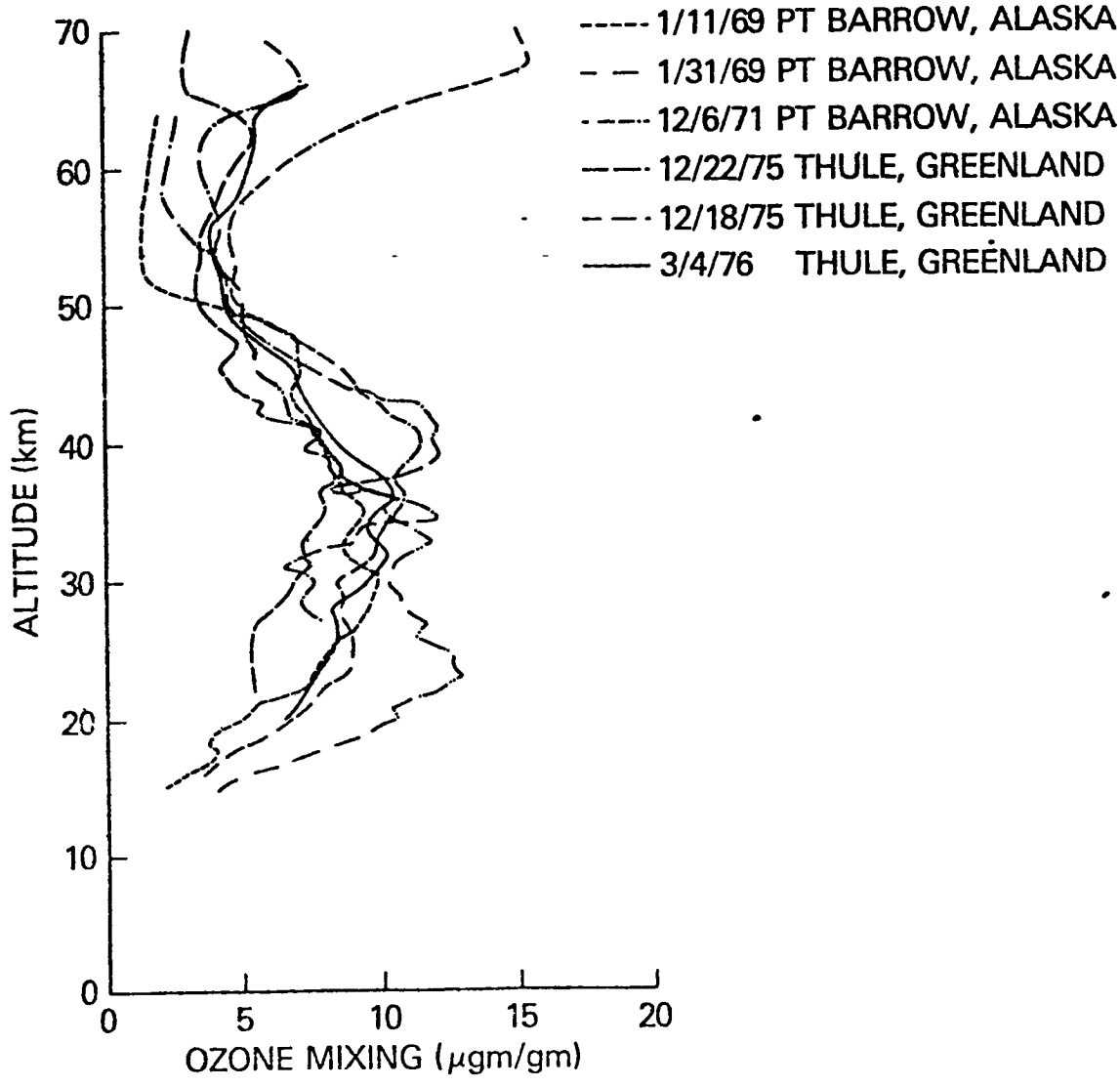

Figure 12 Ensemble of ozone profiles obtained during the polar night

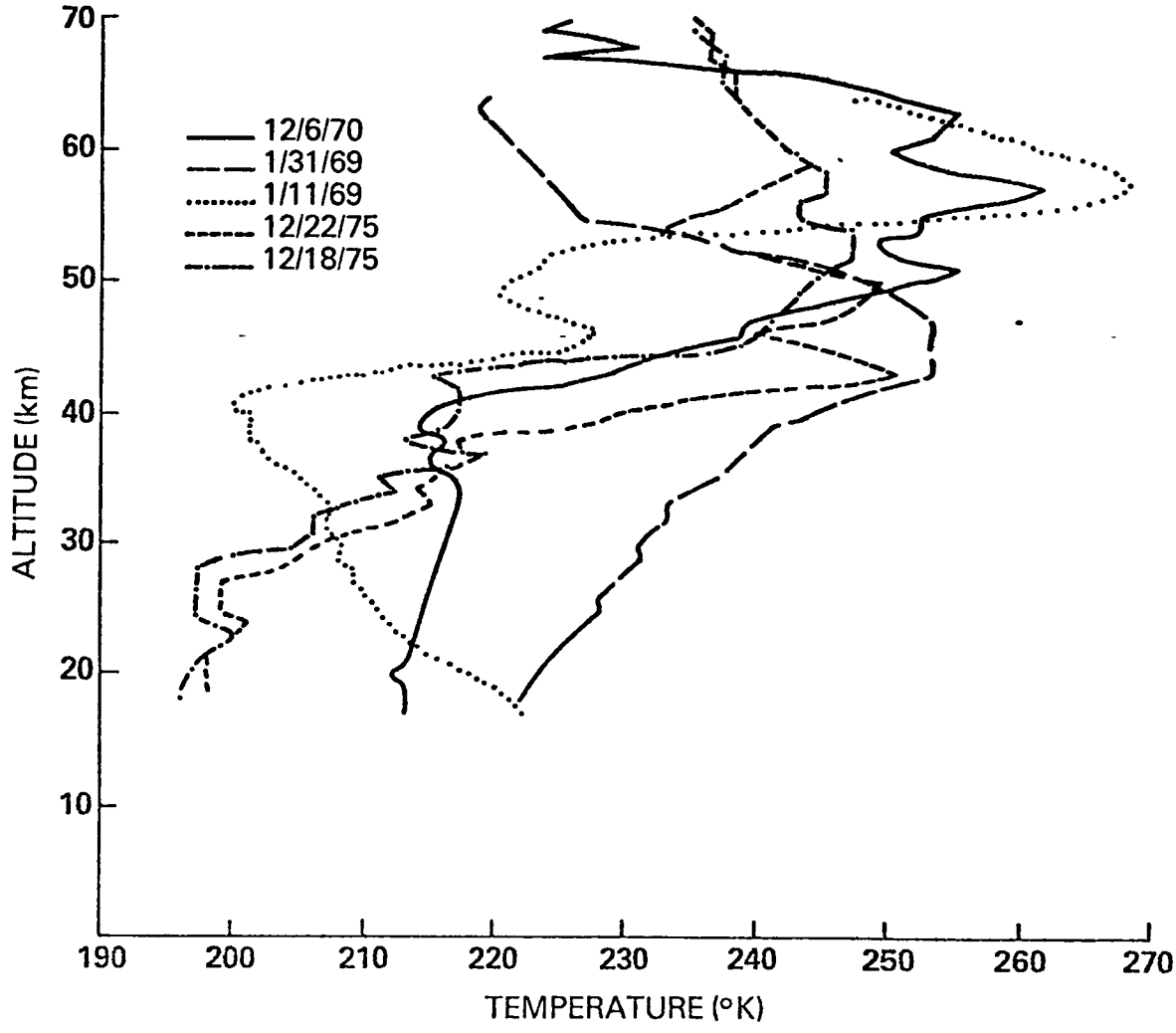

Figure 13 Temperature profiles measured at same time as the ozone profiles shown in Figure 11

For the January 1969 flights in Alaska the winds were generally westerly from 30 to 80 km However, above 55 km, on January 11th, the winds were from the northwest, and on the 31st they were from the southwest, because of the displacement of the polar vortex toward Siberia resulting in anticyclonic flow near Alaska above 50 km Therefore, on the former flight, air above 55 km originated from polar regions and on the latter flight, from sunlit regions. To some degree the changes are explained by the temperature changes alone, as mentioned above, however, changes in temperature could also result from vertical motions as well as from advection. At the time of the December 1971 flight, which showed unusually large ozone amounts above 60 km, the polar vortex at 10 mb caused westerly winds over northern Alaska The westerly wind persisted to about 60 km and then became northerly above this level. This would indicate an eastward displacement of the polar vortex and anticyclonic flow in the upper mesosphere, bringing air from higher latitudes or altitudes over northern Alaska.

Upper level meteorological data from the 1975-1976 winter are more complete than for 1969 and 1971. Unfortunately the ozone soundings conducted from Thule, Greenland, on December 18 and 22, 1975, and March 4, 1976 were not near the time of the significant warming that occurred over the Northwest Atlantic during the second week of January 1976 revealed by the National Weather Service (NWS) (30) However, in the week containing the December 18 and 22 soundings, there were minor temperature anomolies over Greenland as the polar vortex oscillated over, and about, the pole (30) Below 50 km the winds became more northerly between the 18th and 22nd and the temperature increased by about 10°C. while the ozone decreased about 50% This is a large change in a short period, but is consistent with the earlier observations Above 50 km the ozone profiles are about the same where both show slightly increasing mixing ratios with altitude The profile observed on December 18th shows an unusually sharp decrease in ozone between 35 and 38 km never previously

observed This feature can be correlated with a minor discontinuity in the corresponding temperature profile (temperature and wind data are measured independent of the ozone profile), however, a measurement error cannot be discounted. The significant warm anomaly that appeared in the second week of January in the North Atlantic can be first detected in late December, when the temperatures at 50 km rose nearly 10°C (29). Perhaps the unusual feature in the ozone profile was caused by a local disturbance that was a precursor to the January event. The next ozone sounding at Thule was conducted in early March 1976 During the winter months the vortex did not break down and the high latitude anticyclone did not develop until late March. The meteorological sounding accompanying the ozone sounding showed northerly winds from 30 to 50 km and winds southwesterly above this level A well-defined stratopause appeared and the ozone profile had a typical midlatitude spring characteristic, with a distinct mixing ratio peak near 38 km of about 12μ gm/gm. The ozone measurement was performed at night which accounts for the mixing ratio increase from 5 to 9μ gm/gm from 55 to 65 km.

The ozone soundings described here give only snapshots of the complex dynamic and chemical behavior of the upper atmosphere during the polar night An adequate description of the ozone behavior is not possible without detailed information on the transports and the distribution of other atmospheric species important in ozone chemistry No synoptic upper air data above 10 mb are available for the Alaska ozone soundings The weekly upper air analyses from the NWS (30) for the winter of 1975-1976 help a great deal, but during the winter months there are observed day-to-day changes in the temperature and pressure height fields that most likely affect the ozone distribution. Finally, there is no information on the distribution of other chemically active gases during the polar night. These data have shown, however, that the ozone distributions are highly variable, but, within a factor of two, when compared to distributions at lower latitudes, and to some degree can be explained by the temperature and the wind fields

VII. Conclusions and Summary

The chemiluminescent principle for in-situ ozone observations in the stratosphere and mesosphere was reviewed. The measurement principle employs chemiluminescence in a parachute drop sonde, where the air is sampled by a passive pumping system. Laboratory measurements have shown a linear relationship between the chemiluminescence and ozone flux at the low flow rates and pressures encountered during a parachute descent. The chemiluminescence is sensitive and specific to ozone and has suitable stability for routine rocket measurements.

The sonde has been engineered for flight on a Super Arcas meteorological rocket The sonde is ejected near apogee (75 km) and descends on a special parachute, which provides sufficient drag and stability for high altitude performance. The chemiluminescent detector consists of Rhodamine-B dye adsorbed on a porous glass substrate. The chemilumescence is monitored by a stable photometer, while the flow is derived from pressure and temperature measurements inside a ballast chamber at the end of an air inlet pipe. The ozonesonde employes a pulse code modulated (PCM) telemetry system using the 1680 MHz meteorological carrier frequency.

Each ozone sensor is calibrated several times prior to flight to determine its sensitivity to ozone The calibration device consists of a vacuum apparatus and fills with an air ozone mixture with the ozone sensor attached Calibration is accomplished by exposing the sensor to known ozone amounts, flow rates, and pressures expected in flight The ozone content is determined by a laboratory ozone monitor calibrated against an NBS standard utilizing an absorbtion cell at 253 7 nm.

An error analysis was performed by classifying the experiment uncertainties into 1) random errors, 2) flight-to-flight systematic errors, and 3) experiment errors which involve the absolute

accuracy The first error, due to noise, and the second, due to undetected biases in the sensor subsystems, were combined to yield a measurement precision of 8%. Two flights conducted nearly simultaneously resulted in a repeatability of about 6%, which very well supports the calculated precision The third error is most difficult to assess, however, comparisons with rocket optical sondes and a single coincident LRIR sounding from Nimbus-6 resulted in differences between 5 and 20% in the ozone profiles. This results supports the overall measurement accuracy of 14% computed from the combined precision and absolute error.

Beginning in 1968 ozone profiles were measured under varying geophysical conditions with emphasis on measurements during the night. The early soundings were used for the initial verification of photochemical models which predicted ozone depletion. Diurnal variations measured at low and midlatitudes showed some latitude dependence. Daytime measurements were used in the Krueger-Minzner empirical model. They also result in ozone concentrations in the upper stratosphere and mesosphere considerably higher than those calculated from one-dimensional models with fairly complete chemistry However, equatorial nighttime ozone distributions measured by the chemiluminescent sonde are significantly lower than nighttime equatorial ozone distributions obtained from satellite ultraviolet stellar occultation measurements Ozone distributions were also obtained during the polar night under varying wind and temperature conditions These profiles had considerably more variations when compared to stratospheric and mesospheric ozone profiles at lower latitudes To some degree, the ozone variability was explained by the large variations in the temperature and winds that occur during winter at high altitudes However, the ozone behavior is difficult to explain without detailed information on the transports and the distribution of other atmospheric species that are important in ozone chemistry

REFERENCES

1. Krueger, A. J , W. R. McBride, Rocket Ozonesonde (ROCOZ) Design and Development, Naval Weapons Center Report TP 4512, 1968.

2. Randhawa, J. S., Ozonesonde for Rocket Flight, *Nature*, 213, 1967, pp. 53-54.

3. Weeks, L. H., L. G. Smith, A Rocket Measurement of Ozone Near Sunrise, *Planet Space Sci*, 16, 1968, pp. 1189-1195.

4. Hilsenrath, E., L. Seiden, P. Goodman, Ozone Measurement in the Mesosphere and Stratosphere by Means of a Rocket Sonde, *J. Geophys Res* , 74, 1969, pp. 6874-6880.

5. Nagata, T., T. Tohmatsu, and T. Ogawa, Sounding Rocket Measurement of Atmospheric Ozone Density, 1965-1970, *Space Research, 11*, Akademie, Berlin, 1971, pp. 849-855.

6 Llewellyn, E. J. and G. Witt, The Measurement of Ozone Concentrations at High Latitude during Twilight, *Plant Space Sci*, 25 Pergamon Press, 1977, pp. 165-192.

7. Carver, J. H., B. Horton, and F. G. Burger, Nocturnal Ozone Distribution in the Upper Atmosphere, *J Geophys Res* , 71, 1966, pp 4189-4191.

8. Subbaraya, B. H , S Lal, Rocket Measurements of Ozone Concentrations in the Equatorial Stratosphere at Thumba, preprint from *Space Research, 19*, COSPAR paper VI.4.9, 1978

9. Stolarski, R S., The Impact of Chlorofluoromethane and NO_x Injections on Stratosphere Ozone, Proceedings of the 4th Joint Conference on Serving of Environmental Pollutants, American Chemical Society, 1978, pp 20-26

10. Wright, D. U , A J Krueger and G M Foster, Rocket Ozone Sounding Network Data, Quarterly Report, NASA TM 69365, December 1978

11 The Nimbus 7 User's Guide, prepared by the Landsat/Nimbus Project Goddard Space Flight Center, NASA, August 1968

12 Beranose, H J , and M G Rene, Oxyluminescence of Few Fluorescent Compounds of Ozone, *Ozone Chemistry and Technology, Advan Chem Ser* , 21, 1959, pp. 7-12

13 Regener, V H , Measurement of Atmospheric Ozone with the Chemiluminescent Method, *J Geophys Res* , 69, 1964, pp 3795-3800

14 Herring, W S and H U Dütsch, Comparison of Chemiluminescent and Electrochemical Ozonesonde Observations, *J Geophysical Res* 70 No 22, 1965 pp 5438-5490

15 Komhyr, W D , R D Gross R A Proulx Ozonesonde Intercomparison Test, ESSA Technical Report, ERL 85-APCL 4, September 1968

16 Panametrics, Studies of the Reaction between Ozone and a Chemiluminescent Disk, Final Report NASA 5-11502 to Goddard Space Flight Center, February 1971.

17. Hodgeson, A., K. J Frost, A E. O'Keefe, and R K Stevens, Chemiluminescent Measurement of Ozone, Response Characteristics and Operating Variables, *Analytical Chemistry*, 42, pp 1975-1802.

18 Seiden, L., Panametrics, Final Report F. 19(628) 315 to Air Force Cambridge Research Laboratories, 1962.

19. Bersis, D. and E. Vassiliou, A Chemiluminescence Method for Determining Ozone, *Analyst*, 91, August 1966, pp. 499-505.

20 Steinburger, E. H , J Sivan, T. Newmann, N. W. Rosenberg, Laboratory Analysis of Chemiluminescent Ozone Measurements, *J Geophys Res*, 72, 1967, p. 4579.

21. Hudson, R. D. (ed), Chlorofluoromethanes and the Stratosphere, NASA Reference Publication 1010, August 1977.

22. Hilsenrath, E., Ozone Measurements in the Mesosphere and Stratosphere during two Significant Geophysical Events, *J Atmos Sci*, 28, 1971, pp. 295-297.

23 Heath, D F., E. Hilsenrath, A. Krueger, W. Nordberg, C. Prabhakara, and J. S. Theon, Observations of the Global Structure of the Stratosphere and Mesosphere with Sounding Rockets and Remote Sensing Techniques from Satellites, *Structure and Dynamics of the Upper Atmosphere*, F. Verniani (ed.) Elsevier Publishing Co , 1974.

24. Goldberg, R. A., and E Hilsenrath, Operation Aurorozone An Experiment in Sun/Weather, Proceedings of the Third NASA Weather and Climate Review, NASA Conference Publication 2029, E. J. Kreins (ed.), November 1977.

25. Krueger, A. J. and R A Minzner, A Midlatitude Ozone Model for the 1976 U.S. Standard Atmosphere, *J. Geophys. Res*, 81, 1976, p 4477

26. Watanabe, T. and T Tohmatsu, An Observational Evidence for the Seasonal Variation of Ozone Concentration in the Upper Stratosphere and Mesosphere, *Report of Ionosphere and Space Research in Japan*, 30, 1976, pp. 47-50

27. Butler, D. M , The Uncertainty in Ozone Calculations by a Stratospheric Photochemistry Model, *Geophysical Research Letters, 5*, No. 9, September 1978, pp. 769-772.

28 Riegler, G. R , Atreya, S. K., T. M Donahue, S C. Liu, B. Wasser, J. F. Drake, UV Stellar Occultation Measurements of Nighttime Equatorial Ozone, *Geophysical Research Letters*, 4, No 4, April 1977, pp 145-148

29 Kuhn, W. R , D Kraemer, R J Cicerone, S Lin, Radiative Equilibrium Temperatures in the Stratosphere and Mesosphere—A Comparison for the Stellar Occultation and BUV Ozone Data, *Geophysical Research Letters, 5*, No 5, May 1978, pp 365-368

30 Synoptic Analysis, 5-, 2-, and 0 4 Millibar Surfaces for July 1974 through June 1976, Prepared by Upper Air Branch, NOAA, National Weather Service, NASA Reference Publication 1023, June 1978

APPENDIX A

OZONE DETECTOR PREPARATION

1 Dissolve Vycor® 7930 disc in a hot 10 percent sodium hydroxide solution to desired thickness, or until glass becomes clear The Vycor® material will turn milky upon immersion in the solution.

2 Wash the glass thoroughly in hot water until disc yields a neutral reaction to Ph indicator paper

3 Dry discs under ambient conditions until transparent. Heat in an oven at 110°C

4 Dip the disc into a solution of 2 mg gallic acid and 0 4 mg rhodamine-B per 1 ml of acetone for 10 minutes

5 Dry in air and store discs in a dark desiccator until used.

APPENDIX B

BLACK ANODIZE PROCEDURE

1 Cleaning

a Vapor degrease parts using a degreasing compound that contains no silicones.

b Light etch parts with either nitric acid or nitric hydroflouride acid.

2 Anodizing

a One (1) hour in a 15 percent solution of sulfuric acid at 70° to 75° F at 15 volts.

3 Dyeing

a Mix sandoz fast black type O A (or equivalent) 10 grams per liter.

b Dye for 20 minutes at solution temperature of 140° to 150°F.

4 Sealing

a Nickel acetate with buffers (sandofix or equivalent)

b Seal for 20 minutes at 190°F

5 Packaging

a Immediately after sealing place parts in plastic bag to prevent contamination.

APPENDIX C

"L" BAND PULSE CODE MODULATION (PCM)

TELEMETRY UNIT AND POWER SUPPLY

1 Physical Characteristics

The battery pack consists of 6 Yardney HR 1.5 silver cell batteries housed in the sensor portion of the sonde. The telemetry system weighs 408 grams, is 10 centimeters in diameter and 15 centimeters long.

The RCA cavity tube and plates are potted with RTV 106 while the converter transformer is potted with Wakefield Engineering Delta 153-2 with 153-2 type RTA-2 hardener. The overall unit including antenna, except batteries, is potted with Ecofoam FPH with catalyst 12-24.

Printed circuit boards are used throughout. The PCM system is depicted, attached to ozone sensor, in Figure 3 of this report.

2 Power

The telemetry and sensor units require several supply voltages, including ±15 VDC, +6 VDC, and +115 VDC, all derived from the onboard DC-to-DC converter which is powered by the 9 volt battery supply Converter conversion efficiency is about 76%. The DC to DC converter will function efficiently down to 7.6 volts at the input

3 PCM Encoder

Flat Pack Cmos integrated circuits are used to minimize both power and size Ramp or countdown type A/D converters are used The analog-to-digital converter is eight bit and the encoder is adjusted for 125 counts, which equals 2.50 volts from the sensor. Digital resolution is 20 millivolts. There are nine words per frame or eight data words and one sync word Bi-phase modulation is used The encoder analog impedance is 10 megohms and analog inputs should not exceed −3 and

+10 VDC The main crystal controlled oscillator is 2.045 MHz with a clock rate of 512 kHz for A/D conversion The bit rate is 8kHz (512/64) This gives a word rate of 100 per second or frame rate of 11 per second

4 Environment

The telemetry and power supply unit are tested and monitored through a temperature range of −40 to 70 degrees centigrade. Voltage breakdowns in vacuum are checked The units survive a range of vibration loads and shock of 100g's for 2 milliseconds.

5 Interface connectors

The umbilical connector provides battery check, external power, and internal/external power transfer functions. There is an interstage connector between the ozone sensor and telemetry power unit. RF power turn-off is accomplished with a specially designed shorting connector while the remainder of the telemetry continues to function This allows the encoder outputs to be brought out for sensor checks without R F radiation

An interface block diagram of the sensor and telemetry-power unit is shown in Figure C-1.

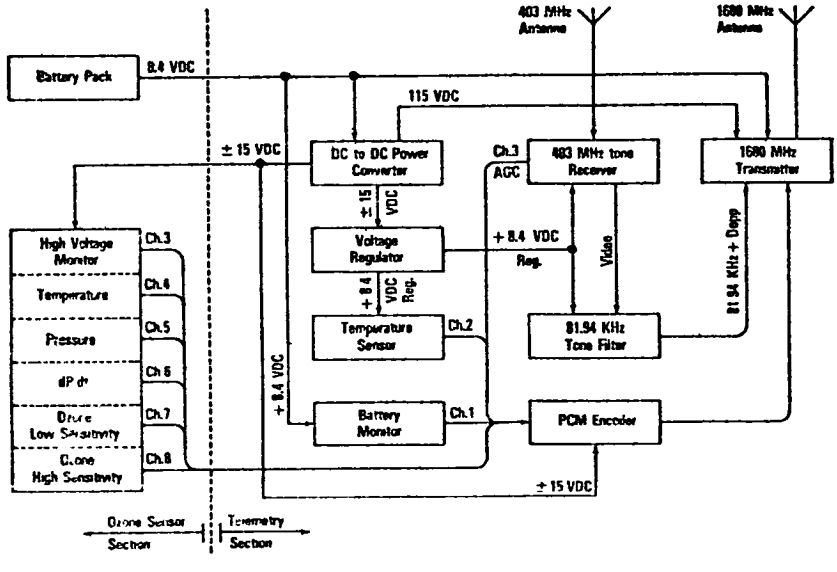

Figure C-1. Block diagram of telemetry system components and interface with ozone sensor

End of Document